Arabian Journal of Geosciences (2022) 15: 601
https://doi.org/10.1007/s12517-022-09898-3

ORIGINAL PAPER

Estimation of aboveground forest biomass in Himalayan region of West Bengal, India using IRS P6 LISS-IV data

Kaushik Ghosal[1] · Santasmita Das Bhattacharya[1] · Prabir Kumar Paul[1]

Received: 22 January 2021 / Accepted: 15 March 2022 / Published online: 24 March 2022

Abstract
Forest aboveground biomass (AGB) measurement is a direct estimator of the live carbon stock of that forest region. Increasing emission and concentration of CO_2 is a global threat as it is a major cause of today's global warming. The forest AGB is a live carbon sequester that plays a major role by absorbing atmospheric CO_2. There are field-based measurement methods of AGB, but the main disadvantage is that they are primarily destructive. Several authors have undertaken AGB estimation using different remote sensing data types, but they are mostly not cost-effective for extensive study areas. We have created a cost-effective algorithm for AGB estimation using multispectral (MSS) data. In this study, Indian Remote-Sensing Satellite-P6 (IRS P6) Linear Imaging Self-Scanning Sensor-4 (LISS-IV) MSS data have been used for the analysis. The research has tried to estimate the AGB of different types of forests existing in the study area by using various vegetation indices and the gray-level co-occurrence matrix (GLCM) and created a hybrid methodology combining the vegetation indices and GLCM. Among all vegetation indices, the simple ratio (SR) highly correlates with AGB of pure deciduous and coniferous forests. In a mixed forest region, due to a mixture of two canopy stands, there is a mixture of foliage angle and optical scattering distribution. Therefore, modified simple ratio (MSR) becomes dominant in mixed forest AGB estimation. Previously there was no study to justify this GLCM texture parameter selection. In this study, we have justified the parameter selection of GLCM texture statistics. This parameter selection will help researchers choose the proper GLCM texture parameter for their study. Integration of GLCM textures with vegetation indices enhances the AGB model strength for all forest regions. The deciduous forest map gives validation R^2 of 0.89 with an RMSE of 1.93 ton/pixel. The validation R^2 of the Coniferous Forest map is 0.83 with an RMSE of 1.35 ton/pixel. There is a comparatively identifiable improvement in mixed forest with validation R^2 of 0.96 and RMSE of 0.25 ton/pixel. This study shows AGB storage of deciduous forest has a maximum share over other forest region of Kalimpong forest.

Keywords Gray-level co-occurrence matrix · Aboveground biomass · Optical remote sensing · Vegetation indices · Entropy

Introduction

Greenhouse gases are a significant contributor to global warming. Among all other greenhouse gases, CO_2 contributes the most to global warming. The forest AGB is a live sequester of emitted CO_2. The assessment of forest aboveground biomass (AGB) is an essential part of national development planning as it incorporates the productivity of an ecosystem, carbon budget, and etc. (Parresol 1999; Zianis & Mencuccini 2004; Zheng et al. 2004; Hall et al. 2006). In addition to the economic aspect, it dramatically impacts global climatic variables.

Field-based AGB measurements were the standard methods for AGB estimation of a forest area. The field-based methods were mostly destructive and not practicable in a

Responsible Editor: Biswajeet Pradhan

✉ Kaushik Ghosal
kaushikghosal02@gmail.com

Santasmita Das Bhattacharya
santasmita@gmail.com

Prabir Kumar Paul
prabirpaul59@gmail.com

[1] Department of Mining Engineering, Indian Institute of Engineering Science and Technology, Shibpur, West Bengal, India

mountainous terrain where most of the area is inaccessible. Remote sensing has been mainly used to estimate forest AGB as it is more economical and less time-consuming to measure the AGB of a forest than field-based estimation. Remote sensing methods are the only way to assess the AGB of forests in hilly terrain with inaccessible tracts of land parcels.

Researchers have studied different remote sensing approaches. These approaches are majorly divided into two parts: (1) optical or passive remote sensing and (2) active remote sensing approach. In the active remote sensing-based approach, researchers have mainly focused on the synthetic-aperture radar (SAR)-based approach for monitoring AGB. Among all SAR data, only L band data have penetration capability through the surface canopy layer and then get scattered back by the trunk and main branches (Blomberg et al. 2018). The L band data to be used should have to be cross-polarized (i.e., HV or VH) as cross-polarized data can give the volumetric backscatter (Xiang et al. 2016) from the tree trunks and branches that have a reasonable correlation with the AGB of that forest (Luckman et al. 1997; Kurvonen et al. 1999; Sun et al. 2002; Günlü and Ercanlı, 2020). Although the L band cross-polarized data have a reasonable correlation with forest AGB, temporal measurements of AGB at a specified period are very costly and uneconomical. The researchers have studied optical data to estimate forest AGB to make the estimation more economical. Multispectral and hyperspectral optical data have been used to estimate forest AGB by different researchers all over the globe. Although hyperspectral data demonstrates some AGB estimation successes, the data suffers from the problem of band redundancy. The application of hyperspectral data is significantly less in AGB estimation because of its minimal availability (Hyperspectral data are mainly airborne and captured in small areas) (Lu et al. 2016).

Multispectral (MSS) data are the most used data for forest AGB assessment among all other remote sensing data due to the availability of its various spatial, spectral, radiometric, and temporal resolutions. There are various MSS data available like Landsat-5 TM (Roy & Ravan 1996; Wylie et al. 2002; Foody et al. 2003; Phua & Saito 2003; Lu 2005; Lu et al. 2005 (a); Du et al. 2012; Singh & Das 2014; Günlü et al. 2014; Barrachina et al. 2015; Das & Singh 2016), Landsat-7 ETM+ (Zheng et al. 2004; Avitabile et al. 2012), Landsat-8 OLI (Ali et al. 2018; Li et al. 2018), Sentinel-2 (Askar et al. 2018; Ali et al. 2018; Pandit et al. 2018; Keleş et al. 2021), and LISS-3 (Kumar et al. 2013; Mayamanikandan et al. 2017; Nandy et al. 2017), Aster (Fuchs et al. 2009). Due to free availability and good spectral resolution, Landsat series and Sentinel 2 are the most commonly used MSS data for forest AGB estimation. Although the spatial resolution of Sentinel 2 data does not meet the accuracy required in the estimation of forest AGB, researchers are also using the high-resolution MSS data like IKONOS (Thenkabail et al. 2004; Kayitakire et al. 2006), Quickbird (Fuchs et al. 2009; Sousa et al. 2015), Worldview (Obeyed et al. 2018), GeoEye (Mareya et al. 2018), and RapidEye (Gascón et al. 2019) for estimation of forest AGB. Due to high-cost involvement and lack of availability of IKONOS data, it is challenging to identify the AGB of a forest where regular monitoring is required at a specific interval of time.

Previously, a few studies on AGB estimation have been done by some researchers using Linear Imaging Self-Scanning Sensor-4 (LISS-IV). Madugundu et al. (2008) used LISS-IV data to estimate AGB by leaf area index (LAI) determination and got an R^2 value of 0.63 between the estimated and field-observed AGB of Haliyal and Yellapur Forest Divisions, Western Ghats of Karnataka, India. On the other hand, Pargal et al. (2017) studied the AGB of different forest types of Yellapur Forest Division, Uttara Kannada District, Western Ghats of Karnataka, India, with LISS-IV. He used the vegetation index, NDVI, for his analysis. He got $R^2 = 0.82$ for his AGB model. Attri and Kushwaha (2018) have used LISS-IV data on Barkot Forest Range, Dehradun, India. For identification of AGB using NDVI, he got $R^2 = 0.71$ for his AGB model.

Very few studies apply gray-level co-occurrence matrix (GLCM) texture parameters on AGB estimation. Lu and Batistella (2005) and Lu (2005) have used eight textural parameters of Landsat-5 TM data to identify AGB and got maximum $R^2 = 0.68$ and 0.71, respectively. Kayitakire et al. (2006) have used GLCM of IKONOS data. He got an R^2 value of 0.82. This work indicates that high-resolution GLCM textures have a high correlation with forest AGB. For AGB estimation, some researchers have integrated both vegetation indices with the GLCM texture. Lu (2005) has used the integrated model with Landsat-5 TM data and got $R^2 = 0.77$. Fuchs et al. (2009) have used coarse resolution ASTER data and high-resolution Quickbird data and got $R^2 = 0.63$ and 0.69, respectively. Avitabile et al. (2012) had used Landsat-7 ETM+ data and got $R^2 = 0.81$. Nandy et al. (2017) had used LISS-3 data and got $R^2 = 0.746$. Gascón et al. (2019) had used RapidEye data and got $R^2 = 0.69$ for their AGB models.

The forest region of Kalimpong has dense forest cover. There is no study available on the estimation of AGB of Kalimpong forest. Due to a gradual increase in human habitation, deforestation is a significant concern for these forests. In addition to this, monitoring of AGB is one of the essential measures to identify forest health. Kalimpong is hilly terrain, with most places inaccessible for collecting physical measurements of forest AGB due to stiff slopes. Not only stiff slopes but several reserve forests, protected forests, and Indian army-occupied forest regions are not permitted entry due to government rules. Therefore, physical identification and forest inventory-based sample collection are challenging in the Kalimpong forest region. For delineating these problems of the study area, this research attempted to identify a cost-effective method for AGB estimation, which can be used by the authorities for the measurement of AGB periodically. In this work, MSS data that is IRS P6 LISS-IV, which is a meager cost high-resolution data, have been used to create a cost-effective, accurate methodology for estimating AGB. There are few studies on AGB estimation using vegetation indices of high-resolution LISS-4 data. However, no study is available on the relationship of GLCM-based texture parameters of LISS-4 bands with AGB of the forest. There is no study on the impact of forest vegetation indices and textures of spectral response with AGB of different forest classes present in Himalayan Forest regions. An attempt has also been made to identify whether the integration of texture and vegetation indices influences the improvement of AGB measurement.

This study has been made to identify the models using LISS-4 generated vegetation indices and GLCM-based texture parameters with AGB of different forest types (coniferous, deciduous, and mixed) of the Kalimpong district. The best fit models have been correlated to come out with models using vegetation indices and the GLCM parameters to increase the accuracy of assessment of AGB of various types of forest in the study area.

Materials and methods

Study area

The Kalimpong district of West Bengal, India is a part of the north-eastern Himalayan region. It lies between 27° 11′ 44″ N to 26° 51′ 40″ N latitude and 88° 23′ 16″ E and 88° 53′ 00″ E longitude. The areal extent of the Kalimpong district is 1095.18 km^2 (Fig. 1). The mean monthly temperature of this area lies between 30 and 9 °C. The annual average rainfall is 2200 mm. The forests under the Kalimpong district mostly fall under the Kalimpong Forest Division of West Bengal Forest Development Corporation (WBFDC), excluding the area under Neora Valley National Park that had been handed over to Wild Life Wing Forest Directorate. The elevation of the study area ranges from 150 to 3700 m. The upper altitude region consists of evergreen alpine coniferous forest, and the lower altitude is covered by temperate deciduous forest. Being a hilly location, most of the forested area is inaccessible, and the accessible places also pose difficulty in collecting the field data. Additionally, shadows of the hills cause many problems in using satellite data in the study area. Only minimal data are available for reliably estimating the existing forest biomass in the Kalimpong district of West Bengal. Deforestation due to the increasing pressure of the growing population and frequent landslides on many forested slopes are affecting the biomass stock in that region, so estimating actual biomass present in that region is necessary to monitor the forests. The detailed methodology flowchart is shown in Fig. 2.

Field inventory data collection and AGB estimation

A total of 59 random sample plots were collected from the different forests of Kalimpong in places that are accessible. There were 18 coniferous forest plots, 26 deciduous forest plots, and 15 mixed forest plots. The field plots were established using purposive sampling (Nesha et al., 2020) due to the constraints of accessibility in the presence of steep slopes and also administrative permissions. *Picea rubens* and *Juniperus virginiana* were the major species found in coniferous forests. In the deciduous forest, the primary species were *Tectona grandis*, *Garuga pinnata*, *Toona ciliate*, *Holarrhena pubescens*, *Albizia procera*, *Shorea robusta*, *Alnus nepalensis*, *Terminalia myriocarpa*, *Quercus pachyphylla*, *Bucklandia populnea*, *Alnus nepalensis*, *Ficus cunia*, *Schima wallichii*, *Michelia champaca*, and etc. The diameter at breast height (DBH), tree height, wood density, and plot area were collected from the field. The details of field inventoried data of the sample areas in coniferous, deciduous, and mixed forests are shown in Table 1.

The field plot distribution has been shown on the LISS-IV MSS data (Fig. 1). The field estimation of AGB has been calculated from this field-collected inventory data.

The AGB was calculated using the volumetric conversion method (Brown & Lugo 1992). AGB density (t/ha) = *F*

$$\text{Aboveground biomass density (t/ha)} = \text{VOB} * \text{WD} * \text{BE} \quad (1)$$

where *VOB* = volume over bark; *WD* = volume-weighted average wood density (tons/m^3 or g/cm^3); and *BEF* = biomass expansion factor (ratio of oven-dry AGB of trees to oven-dry biomass of inventoried volume). (Brown, 1997).

Volume over bark (VOB) has been calculated using the DBH value and the height. Using VOB per hector and volume-weighted average wood density, the biomass of the inventoried volume has been calculated. Biomass expansion factor (BEF) has been calculated using the biomass of the inventoried volume. Volume expansion factor (VEF) has been calculated using the VOB_{30} (i.e., this VOB includes the DBH of trees having a minimum diameter greater than 30 cm) value. VOB_{10} (i.e., this VOB includes the DBH of trees having a minimum diameter greater than 10 cm) has been calculated using the volume expansion factor and VOB_{30}. Finally, AGB has been calculated using VOB10, biomass expansion factor, and volume-weighted average wood density. The AGB in tons/ha of all the 59 plots measured in the field has been calculated using this methodology.

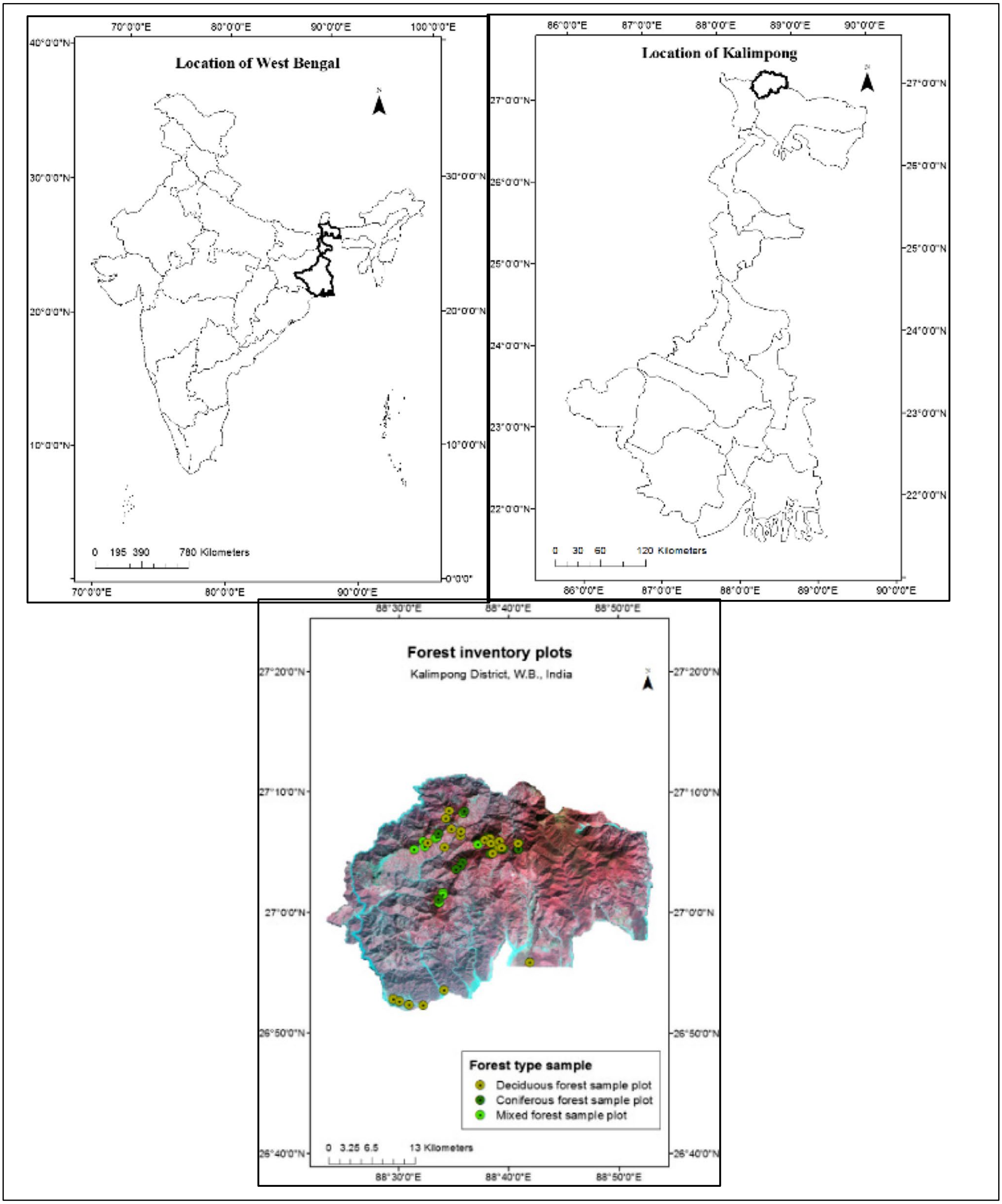

Fig. 1 Study area

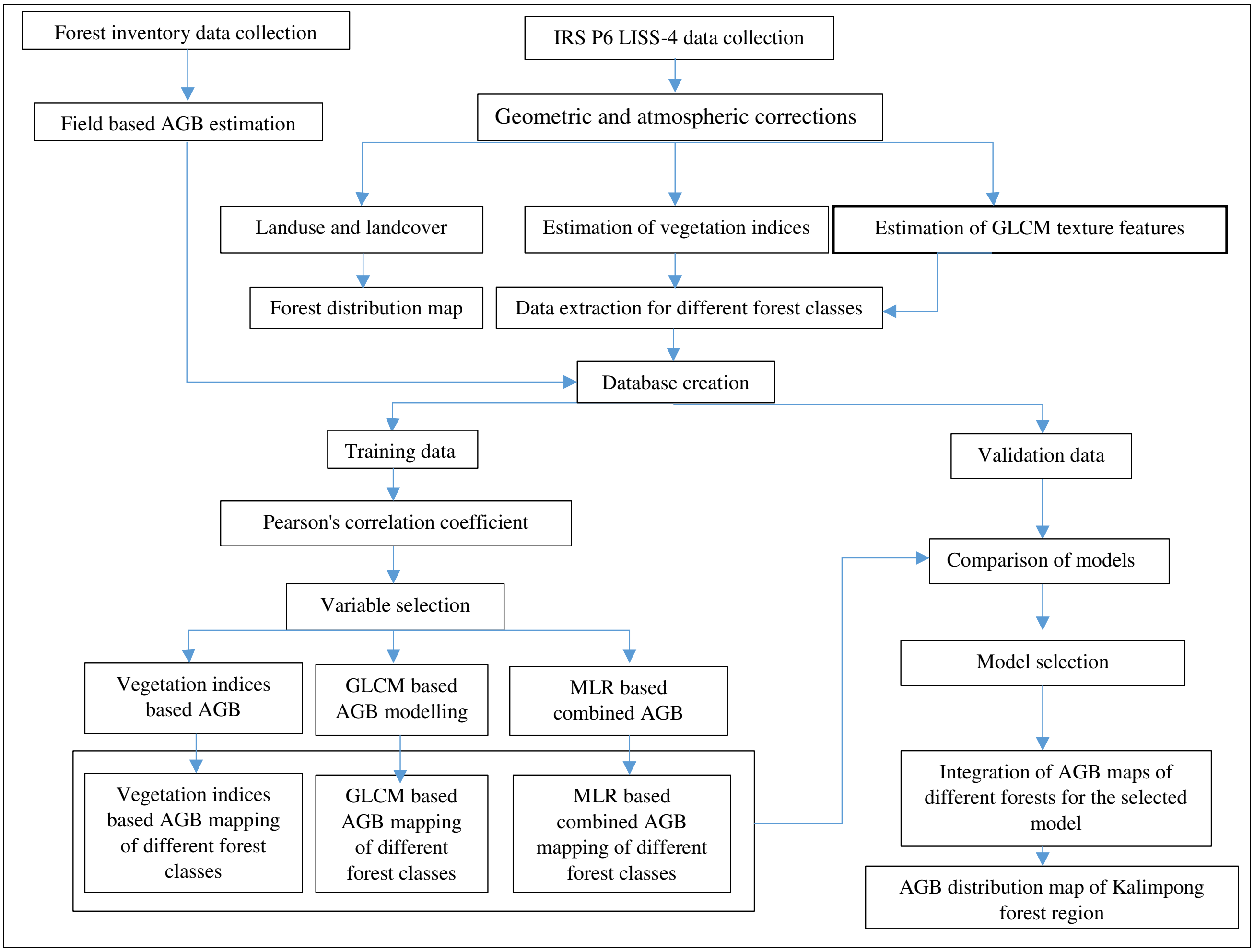

Fig. 2 Methodology flowchart

Table 1 Details of field inventoried data distribution

Forest type	DBH range (cm)	Height range (m)	Wood density range (gm/cc)	Plot area range(m^2)	Tree density range (ha^{-1})	Number of plot
Coniferous forest	12.73–92.30	6.00–22.50	0.375–0.45	95.00–407.17	395.97–1894.17	18
Deciduous forest	11.14–178.25	2.00–30.00	0.255–0.840	50.00–650.98	127.44–1720.43	26
Mixed forest	11.78–133.69	2.00–20.00	0.375–0.840	100.00–625.00	279.27–1324.71	15

Finally, the AGB thus calculated was divided into three classes: coniferous, deciduous, and mixed type of forest for further analysis. It has been found that among 59 plots, there are 18 coniferous forest plots, 26 deciduous forest plots, and 15 mixed forest plots available. We have divided these data into 70% training sample plots (i.e., those sample plots have been used to correlate and model making) and 30% test sample plots (i.e., those sample plots have been used to validate the model).

$$WD = \{(V1/Vt) * WD1\} + \{(V2/Vt) * WD2\} + \ldots\ldots\ldots\{(Vn/Vt) * Wdn\} \quad (2)$$

where V_1, V_2,…. Vn = volume of species 1, 2,.. to the nth species and V_t = total volume WD_1, WD_2,….. Wd_n = wood density of species 1, 2,…… to the *n*th species. (Brown, 1997)

$$BEF = \frac{W_{\text{aboveground}}}{W_{\text{bole}}} \tag{3}$$

where BEF = biomass expansion factor (dimensionless) (Brown, 1997);

$$W\text{aboveground} = W\text{bole} + W\text{crown} \tag{4}$$

where W_{crown} = tree crown dry weight (kg), composed of foliage, thick and thin branches; W_{bole} = tree bole dry weight (kg) (i.e., trunk weight) (Brown, 1997).

$$\left.\begin{array}{l} BEF = e^{\{3.213-0.506*\log(BV)\}\text{forBV}<1\,90\text{t/ha}\}} \\ \quad = 1.74\text{forBV} \geq 190\text{t/ha} \\ \qquad = 1.3(\text{coniferous}) \end{array}\right\}(\text{Deciduous}) \tag{5}$$

where BV = biomass of inventoried volume in t/ha, calculated as the product of VOB/ha (m^3/ha) and wood density (t/m^3) (Brown, 1997).

$$VEF = \frac{VOB_{10}}{VOB_{30}} \tag{6}$$

$$\left.\begin{array}{l} VEF = e^{\{1.300-0.209*\log(VOB_{30})\}} \\ \qquad = 1.13 \end{array}\right\} \begin{array}{l} \text{for}VOB30 < 250\text{m3/ha} \\ \text{for}VOB30 \geq 250\text{m3/ha} \end{array} \tag{7}$$

LISS-IV data accusation

Two cloud-free scenes of IRS P6 LISS-IV were acquired for Kalimpong district from NRSC, Hyderabad, India. Those images were geometrically and atmospherically corrected. LISS-IV data have a swath of 70 km. It consists of three spectral bands: B2 (green (0.52–0.59 mm)), B3 (red (0.62–0.68 mm)), and B4 (NIR (0.76–0.86 mm)). The details of those LISS-IV scenes are given in Table 2. The landuse landcover, forest class map, and vegetation indices of Kalimpong forest have been calculated from this data with the help of the ERDAS Imagine software.

Preparation of forest classification map

The landuse and landcover map has been prepared using a supervised classification based on the field-observed training data points with a maximum likelihood algorithm. The study area has been classified into eight classes: forest, agriculture, waterbody, settlement, barren land, open scrub, tea garden, and sand over the Kalimpong district. Processing of images has been done using a supervised classification based on collected training sets. Among all classes, the forest areas have the maximum coverage of about 817.01 km^2 (about 74.57% of the total Kalimpong district). Other than forest, the agricultural land has coverage of about 89.91 km^2 (8.21%); settlement has coverage of about 89.58 km^2 (8.17%), open scrub has coverage of about 44.77 km^2 (4.08%), waterbody has coverage of about 24.13 km^2 (2.20%), barren land has coverage of about 20.38 km^2 (1.85%), tea garden has coverage of about 9.07 km^2 (0.83%), and the sand deposit has coverage of about 0.73 km^2 (0.066%). The landuse landcover map has been validated using field-collected 191 test datasets. An accuracy of 87.96% and an overall Kappa 0.81 have been achieved for this landuse landcover map (Fig. 3 (a)). The confusion of landuse and landcover distribution is shown in Table 3.

The forest class map (Fig. 3(b)) has been prepared by extracting the landuse classified forest area from the LISS 4 MSS data using a supervised classification of the extracted LISS 4 MSS data. The distribution of forest cover is described in Table 4. The forest map has been validated using field-collected 150 test datasets. An accuracy of 89.33% and an overall Kappa 0.80 have been achieved for the forest map. The confusion of landuse and landcover distribution is shown in Table 5.

Estimation of vegetation indices

From the spectral response curve of the vegetation region, it is identified that the blue and red reflectance is significantly less in the visible spectrum than green. However, there is a sudden increment in reflectance from vegetation beyond the visible range in the infrared region. Red reflectance is sensitive to chlorophyll content, and the near-infrared reflectance is sensitive to the mesophyll structure of leaves. The higher the difference between the red and near-infrared reflectance, the higher the green vegetation present in that pixel. Using this spectral phenomenon of vegetation, researchers have developed several vegetation indices to relate the biophysical parameters of vegetation, like leaf area index,

Table 2 Details of LISS-IV data

Product ID	Path	Row	Sub scene	No. of bands	Date of pass	Shift (%)	No. of band	Spatial resolution (m)
184,811,411	107	052	D	3	12-NOV-2017	0	3	5
184,811,421	107	052	C	3	19-OCT-2017	0	3	5

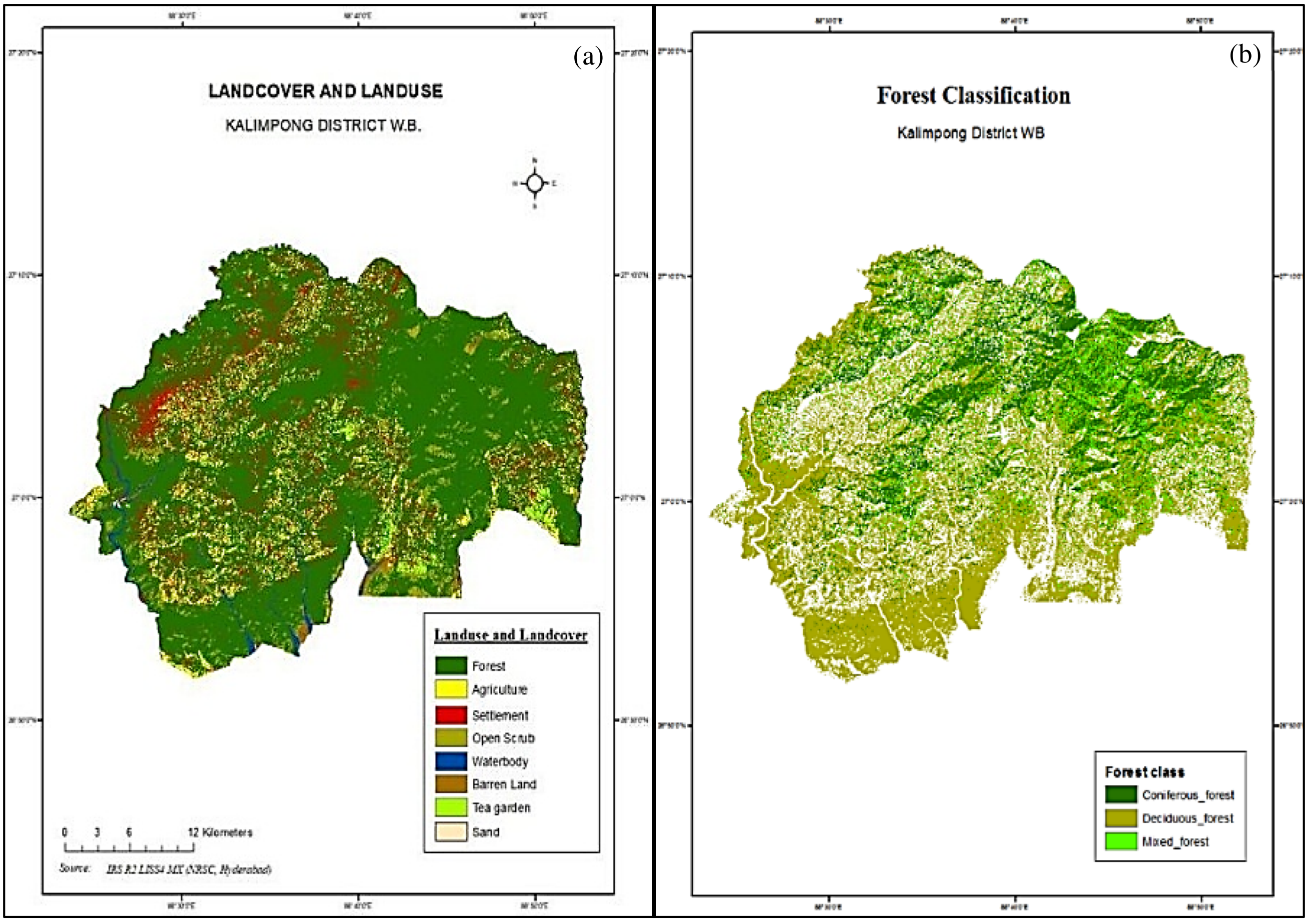

Fig. 3 **a** Landuse landcover map. **b** Forest map.

Table 3 Confusion matrix of landuse and landcover distribution

Reference / Classified	Agriculture	Forest	Settlement	Water body	Barren land	Tea garden	Open scrub	Sand	Reference Totals	Producers Accuracy
Agriculture	12	1	2	0	0	0	0	0	15	80.00%
Forest	6	107	0	0	0	0	0	0	113	94.69%
Settlement	0	0	26	2	0	0	0	0	28	92.86%
Waterbody	0	0	2	5	0	0	0	0	7	71.43%
Barren land	0	0	2	0	3	0	0	0	5	60.00%
Teagarden	0	2	0	0	0	4	0	0	6	66.67%
Open scrub	0	0	0	0	1	2	9	1	13	69.23%
Sand	0	0	0	0	1	0	1	2	4	50.00%
Classified Totals	18	110	32	7	5	6	10	3	191	
Users Accuracy	66.67%	97.27%	81.25%	71.43%	60.00%	66.67%	90.00%	66.67%		

Table 4 Forest distribution of Kalimpong district

Class name	Count	Area (km^2)	Percentage areal cover (%)
Deciduous forest	20,160,389.00	504.01	61.69
Coniferous forest	8,275,128.00	206.88	25.32
Mixed forest	4,245,060.00	106.13	12.99
Total	**32,680,577.00**	**817.015**	**100.00**

percentage vegetation cover, a fraction of absorbed photo-synthetically active radiation (fAPAR), photosynthetic capacity, and carbon dioxide fluxes, and also, they identified a relationship between the forest biomass. In our study, six vegetation indices generated from the high-resolution LISS-IV data have been correlated to measure the AGB of Kalimpong forest. The selected vegetation indices are as given in Table 6.

Table 5 Confusion matrix of forest distribution

Classified \ Reference	Deciduous	Coniferous	Mixed	Reference Totals	Producers Accuracy
Deciduous	72	4	2	78	92.31%
Coniferous	8	56	0	64	87.50%
Mixed	2	0	6	8	75.00%
Classified Totals	82	60	8	150	
Users Accuracy	87.80%	93.33%	75.00%		

Table 6 List of vegetation indices that have been correlated with forest AGB

Indices	Full form	Equation	References
SR	Simple ratio	SR = NIR/RED	Pearson and Miller (1972)
NDVI	Normalized difference vegetation index	NDVI = (NIR – RED)/(NIR + RED)	Rouse et al. (1974)
TVI	Transformed vegetation index	$TVI=(NDVI+0.5)/\lvert NDVI+0.5\rvert*(\lvert NDVI+0.5\rvert)^{0.5}$	Perry and Lautenschlager (1984)
SAVI	Soil adjusted vegetation index	SAVI = 1.5*(NIR – RED)/(NIR + RED + 0.5)	Huete (1988)
RDVI	Renormalized difference vegetation index	$RDVI=(NIR-RED)/\sqrt{(NIR+RED)}$	Roujean and Breon (1995)
MSR	Modified simple ratio	$MSR=(NIR/(RED-1))/\sqrt{(NIR/(RED+1))}$	Chen (1996)

Relationship between AGB of different forests with vegetation indices

The whole field-collected dataset is divided into three major parts according to the forest classification, i.e., deciduous, coniferous, and mixed. Furthermore, the dataset is divided into training (70%) and testing (30%) datasets to establish the model and validate that model. The different vegetation indices are compared to identify the correlation (Pearson correlation) with AGB for each forest class individually. The AGB density has been converted into AGB of each pixel. Those per pixel AGB have been correlated with vegetation index of that pixel generated from LISS-IV data. Plot-wise vegetation index distribution of coniferous, deciduous, and mixed forest AGB are shown in Appendix Tables 22, 23 and 24 respectively. The correlations of vegetation indices with AGB are shown in Table 7.

Among all vegetation indices, simple ratio (SR) has the maximum correlation in coniferous ($r=0.81$) and deciduous ($r=0.75$) forest. In mixed forest, modified simple ratio (MSR) has maximum correlation ($r=0.84$). The relationship between AGB of coniferous, deciduous, and mixed forests is shown in Fig. 4 a, b, and c, respectively.

Estimation of GLCM (gray-level co-occurrence matrix)-based texture parameters

The GLCM-based texture parameters show different combinations of a pixel's gray-level occurrence in an image scene by relating with its neighborhood pixel's gray value.

Table 7 Correlation (r) of different forest AGB with vegetation indices

Forest type	MSR	NDVI	RDVI	SAVI	SR	TVI
Coniferous	0.80	0.79	0.75	0.79	0.81	0.79
Deciduous	0.70	0.62	0.61	0.63	0.75	0.60
Mixed	0.84	0.80	0.74	0.80	0.81	0.80

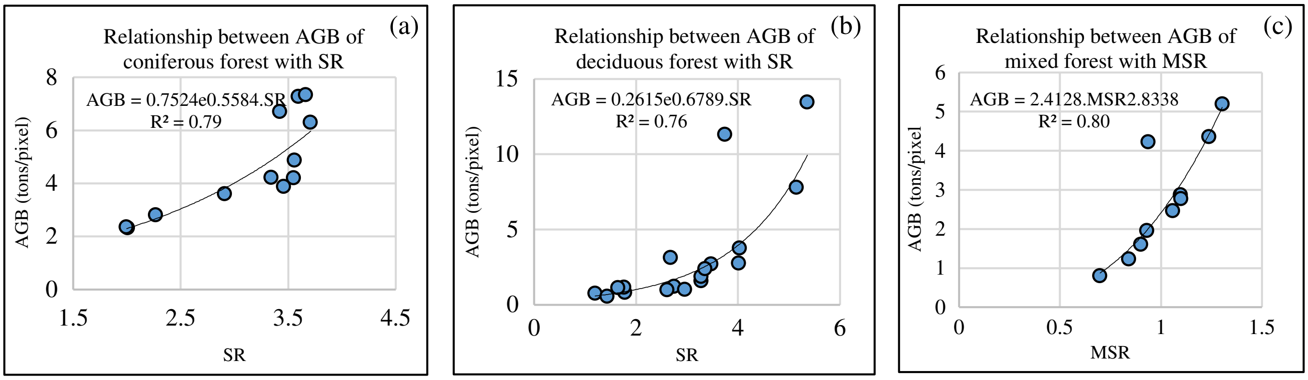

Fig. 4 Relationship between AGB of coniferous (**a**), deciduous (**b**), and mixed (**c**) with vegetation indices

This study generated ten second-order statistics from the GLCM of 3 bands of LISS-4 data (i.e., 30 GLCM texture parameters). Those texture maps have been correlated with the AGB of three different types of forests of Kalimpong. The details of those GLCM second-order statistics are given below (Tables 8 and 9).

The description of notations of the equations given in Table 8 is as follows:

$P(i,j)$ = (i,j)th entry in a normalized gray-tone spatial dependence matrix. (i,j) stands for the number of times gray tones i and j have been neighbors; μ and σ are the mean and standard deviation respectively (Haralick et al. 1973).

Relationship between AGB of different forests with GLCM parameters

The details of training data of coniferous, deciduous, and mixed forest AGB with the all GLCM texture features are in Appendix, Tables 25, 26, 27, 28, 29, 30, 31, 32 and 33. The correlation of AGB with GLCM parameters is given in Table 10. It has been identified that (Table 9) among all GLCM textures, angular second moment of the green band (ASM_GREEN), homogeneity of the red band (HOM_RED), and entropy of infrared band (ENT_IR) have a maximum correlation with AGB of coniferous forest. In the deciduous forest, the entropy of green (ENT_GREEN), red (ENT_RED), and infrared (ENT_IR) has the highest correlation with AGB. Similarly, the contrast of green (CON_GREEN), infrared (CON_IR), and entropy of red (ENT_RED) have the highest correlation with mixed forest AGB.

The relationships between the highest correlated GLCM texture features with AGB of coniferous forest (Fig. 4a, b, c), deciduous forest (Fig. 4e, f, g), and mixed forest (Fig. 5h, i, j) have been chosen for establishing GLCM-based multi-linear regression (MLR) models for estimation of AGB of coniferous forest (Table 11), deciduous forest (Table 12), and mixed forest (Table 13).

Model developed by combining vegetation indices with the GLCM texture parameters

Results

In vegetation index-based models, SR generated models were used for the coniferous and deciduous forests to generate an AGB distribution map of both forests. Similarly, the mixed forest AGB distribution map was generated using the MSR generated model. Those maps have been validated using 30% of the test datasets. The validation plots are shown in Fig. 6a, b, and c for coniferous, deciduous, and mixed forest, respectively.

Among all GLCM-based MLR models, model 7 has the highest R^2 with AGB of coniferous forest (Table 11). Also, deciduous forest model 7 has the highest R^2 (Table 12), and mixed forest model 7 has the highest R^2 (Table 13). Those GLCM-based parameters have been used to generate AGB distribution maps. Those maps have been validated using 30% of the test datasets. The validation plots are shown in Fig. 7a, b, and c for the coniferous, deciduous, and mixed forest, respectively.

The model 7 of the combined model of all forests has the highest R^2 (Tables 14, 15, 16) with AGB. That shows the importance of all the chosen parameters. These combined models have been used to generate AGB maps of each forest. Those maps have been validated using 30% of the test datasets. The validation plots are shown in Fig. 8a, b, and c for the coniferous, deciduous, and mixed forest, respectively.

Table 8 GLCM second-order statistics

2nd order statistical feature	Significance	Formula	Reference
Second moment (ASM)	•Also called uniformity •Measures the pixel pair uniformity that is pair repetition •Detects disorder in texture	$ASM = \sum_i \sum_j i * p(i,j)^2$	Haralick et al. (1973)
Entropy (ENT)	•Measure the disorder and complexity of an image •The entropy is large when the image is not texturally uniform •Complex texture tends to have high entropy •ENT is strongly but inversely proportional with the SEM	$ENT = \sum_i \sum_j i * p(i,j) * \ln(-p(i,j))$	Haralick et al. (1973)
Contrast (CON)	•Measures the spatial frequency of the image pixel and difference moment of GLCM •It is the difference between the highest and lowest values of contiguous set of pixels •It measures the local variations present in the image	$CON = \sum_i \sum_j (i-j)^2 * p(i,j)$	Haralick et al. (1973)
Homogeneity (HOM)	•Also called as inverse distance moment •Measure image homogeneity as it assumes larger values for the smaller gray-tone difference •It is very sensitive to the near diagonal element in the GLCM •HOM decreases when CON increases keeping the SEM constant	$HOM = \sum_i \sum_j \frac{p(i,j)}{1+(i-j)^2}$	Haralick et al. (1973)
Variance (VAR)	•This statistic is a measure of heterogeneity and is strongly correlated to first-order statistical variable such as standard deviation •VAR increases when the gray level of a pixel differs from their mean	$VAR = \sum_i \sum_j \left(i-\mu_i\right)^2 * p(i,j)$	Haralick et al. (1973)
Dissimilarity (DIS)	•Instead of weights increasing exponentially as one moves away from the diagonal as contrast did, dissimilarity weights increase linearly	$DIS = \sum_i \sum_j \lvert i-j \rvert * p(i,j)$	Haralick et al. (1973)
Correlation (COR)	•It passes the calculation of the correlation of a pixel and its neighbor over the whole image means it figures out the linear dependency of gray levels on those of neighboring pixels	$COR = \sum_i \sum_j p(i,j)^2 * \frac{(i-\mu)(j-\mu)}{\sigma^2}$	Haralick et al. (1973)
Maximum probability (MAX)	•This is simply the largest entry in the matrix, and corresponds to the strongest response	$MAX = \max(p(i,j))$	Haralick et al. (1973)
Mean (MEAN)	•Small mean values μd indicate coarse texture having a grain size equal to or larger than the magnitude of the displacement vector	$MEAN = \sum_i \sum_j i * p(i,j)$	Haralick et al. (1973)
Energy (ENG)	• Since energy is used for doing work, thus orderliness •It makes use for the texture that calculates orders in an image	$ENG = \sum_i \sum_j p(i,j)^2$	Haralick et al. (1973)

Table 9 The choice of GLCM property for this study

GLCM property	Selected parameter	Reason
Window size	5×5	Minimum size of window available is 5×5. Increase in window size tends to data loss, so generally minimum window size should be chosen
Direction (θ)	All	Homogeneous class present. As we are doing GLCM for a particular landuse class (i.e., forest)
Quantization level	128	Maximum available in SNAP 7.0. Increase in radiometric resolution implies less loss of gray-level variation and good contrast
Displacement (δ)	2	We are using LISS-4 bands whose pixel size is 5 m and our average plot size is 15.23 m, so in all direction (i.e., horizontal (10 m), vertical (10 m), and diagonal ($10\sqrt{2}$) m), the maximum neighborhood pixel will cover for our plot size

Table 10 Correlation among AGB with all 10 GLCM parameters

Forest class	Bands	GLCM texture features									
		ASM	CON	COR	DIS	ENG	ENT	HOM	MAX	MEAN	VAR
Coniferous	Green	−0.58	0.01	0.00	0.05	−0.56	0.50	−0.52	−0.56	−0.02	−0.04
	Red	0.20	0.15	0.24	0.10	0.20	0.10	0.60	0.55	0.18	0.22
	IR	−0.57	−0.39	0.42	−0.28	−0.60	0.63	−0.46	−0.59	0.20	0.13
Deciduous	Green	−0.57	−0.10	0.10	−0.02	−0.58	0.63	−0.08	−0.37	−0.13	−0.21
	Red	−0.45	0.09	−0.05	0.20	−0.50	0.64	−0.37	−0.36	−0.21	−0.28
	IR	−0.49	−0.06	0.23	−0.08	−0.53	0.59	−0.15	−0.38	0.14	0.12
Mixed	Green	−0.38	0.69	−0.61	0.69	−0.42	0.51	−0.53	−0.18	−0.33	−0.31
	Red	−0.53	0.57	−0.38	0.62	−0.56	0.64	−0.59	−0.51	−0.33	−0.34
	IR	−0.64	0.71	−0.56	0.61	−0.66	0.59	−0.59	−0.68	−0.40	−0.37

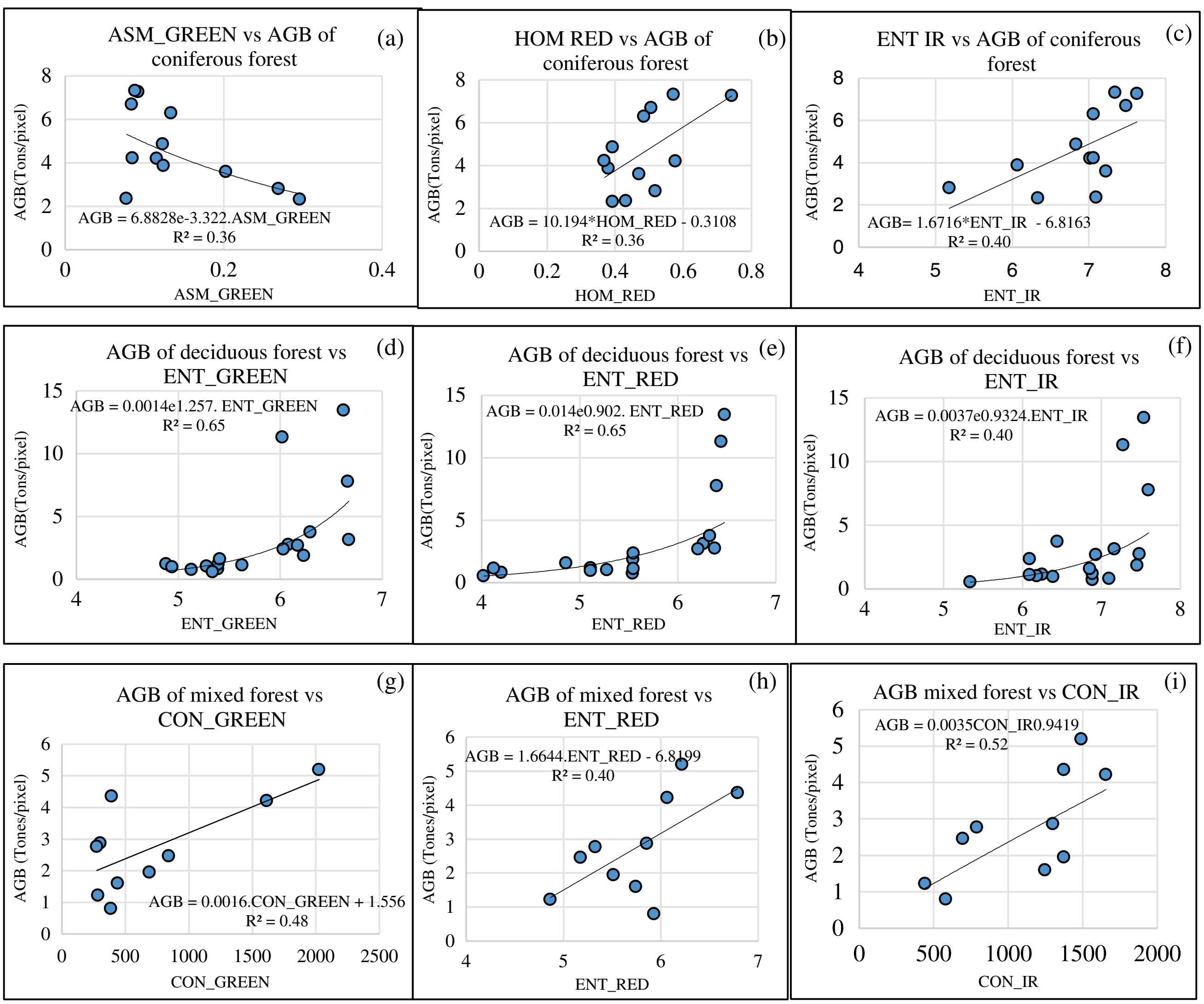

Fig. 5 Relationship between AGB of coniferous forest (**a**-**c**), deciduous forest (**d**-**f**), and mixed forest (**g**-**i**) with GLCM texture features

Table 11 GLCM-based MLR model of coniferous forest

Model	Variable used			Number of variables	Relationship	Model coefficient of determination (R^2)
1	ENT_IR			1	AGB = 1.6716*ENT_IR − 6.8163	0.39
2	HOM_RED			1	AGB = 10.194*HOM_RED − 0.3108	0.36
3	ASM_GREEN			1	AGB = 6.8828*EXP(− 3.322*ASM_GREEN)	0.32
4	ENT_IR	HOM_RED		2	AGB = 0.747852775205543*(1.6716*ENT_IR − 6.8163) + 0.709798271592606*(10.194*HOM_RED − 0.3108) − 2.12726005289109	0.55
5	ENT_IR	ASM_GREEN		2	AGB = 0.722797147512587*(1.6716*ENT_IR − 6.8163) + 0.48894381212065*(6.8828*EXP(− 3.322*ASM_GREEN)) − 0.872661130154658	0.43
6	HOM_RED	ASM_GREEN		2	AGB = 0.840471355012151*(10.194*HOM_RED − 0.3108) + 0.891276320429085*(6.8828*EXP(− 3.322*ASM_GREEN)) − 3.19822262062676	0.56
7	ENT_IR	HOM_RED	ASM_GREEN	3	AGB = 0.416826165533434*(1.6716*ENT_IR − 6.8163) + 0.736781544062229*(10.194*HOM_RED − 0.3108) + 0.566954200560853*(6.8828*EXP(− 3.322*ASM_GREEN)) − 3.22008711022198	0.59

Table 12 GLCM-based MLR model of deciduous forest

MODEL	Variable used			Number of variables	Relationship	Model coefficient of determination (r^2)
1	ENT_RED			1	AGB = 0.014*EXP(0.902*ENT_RED)	0.570
2	ENT_GREEN			1	AGB = 0.0014*EXP(1.257*ENT_GREEN)	0.427
3	ENT_IR			1	AGB = 0.0037*EXP(0.9324*ENT_IR)	0.381
4	ENT_RED	ENT_GREEN		2	AGB = (1.5433980367221*0.014*EXP(0.902*ENT_GREEN)) − 1.44544606367556 + (0.282939580666907*0.0014*EXP(1.257*ENT_RED))	0.577
5	ENT_RED	ENT_IR		2	AGB = (1.46676608709125*0.014*EXP(0.902*ENT_RED)) − 2.17026188620024 + (0.699734945044056*0.0037*EXP(0.9324*ENT_IR))	0.600
6	ENT_GREEN	ENT_IR		2	AGB = − 1.51122384874277 + (0.879675944870026*0.0014*EXP(1.257*ENT_GREEN)) + (1.03958495058038*0.0037*EXP(0.9324*ENT_IR))	0.492
7	ENT_RED	ENT_GREEN	ENT_IR	3	AGB = (1.36808932689061*0.014*EXP(0.902*ENT_RED)) − 2.14064136681706 + (0.126598738500455*0.0014*EXP(1.257*ENT_GREEN)) + (0.654767397041001*0.0037*EXP(0.9324*ENT_IR))	0.601

The detailed model statistics generated from vegetation indices, GLCM, and combined model are discussed in Table 17.

Discussions

The study area is hilly terrain with 74.57% of the forest where most places are inaccessible. There is an urgent need to identify the biomass content of the district. This biomass measurement is for regulatory measures to control the degradation of forests and maintain the forest's health. Keeping this objective in view, this work envisages creating a methodology that will be economical for periodically measuring biomass of the district. There are many options available today for biomass measurement by remote sensing methods, but in this work, LISS-4 data was selected to keep the investigation cost as low as possible.

A few studies were available on the applicability of LISS-4 data as an AGB estimator to date. Madugundu et al. (2008) used LISS-IV generated NDVI to estimate LAI as

Table 13 GLCM-based MLR model of mixed forest

MODEL	Variable used			Number of variables	Relationship	Model coefficient of determination (r^2)
1	ENT_RED			1	AGB = 1.6644.ENT_RED − 6.8199	0.41
2	CON_GREEN			1	AGB = 0.0016.CON_GREEN + 1.556	0.48
3	CON_IR			1	AGB = 0.0035CON_IR$^{0.9419}$	0.53
4	ENT_RED	CON_GREEN		2	AGB = (0.810693126890302*(0.0016*CON_GREEN + 1.556)) + (0.732092547693519*(1.6644*ENT_RED − 6.8199)) − 1.46594719942554	0.68
5	ENT_RED	CON_IR		2	AGB = (0.448356701350558*(1.6644*ENT_RED − 6.8199)) + (0.798423143874*(0.0035*CON_IR^0.9419)) − 0.511750556935335	0.55
6	CON_GREEN	CON_IR		2	AGB = (0.633454237941903*(0.0016*CON_GREEN + 1.556)) + (0.726385062436259*(0.0035*CON_IR^0.9419)) − 0.817943435431242	0.63
7	ENT_RED	CON_GREEN	CON_IR	3	AGB = (0.686568955851643*(0.0016*CON_GREEN + 1.556)) + (0.543699516368457*(1.6644*ENT_RED − 6.8199)) + (0.332029299588111*(0.0035*CON_IR^0.9419)) − 1.45435355281016	0.70

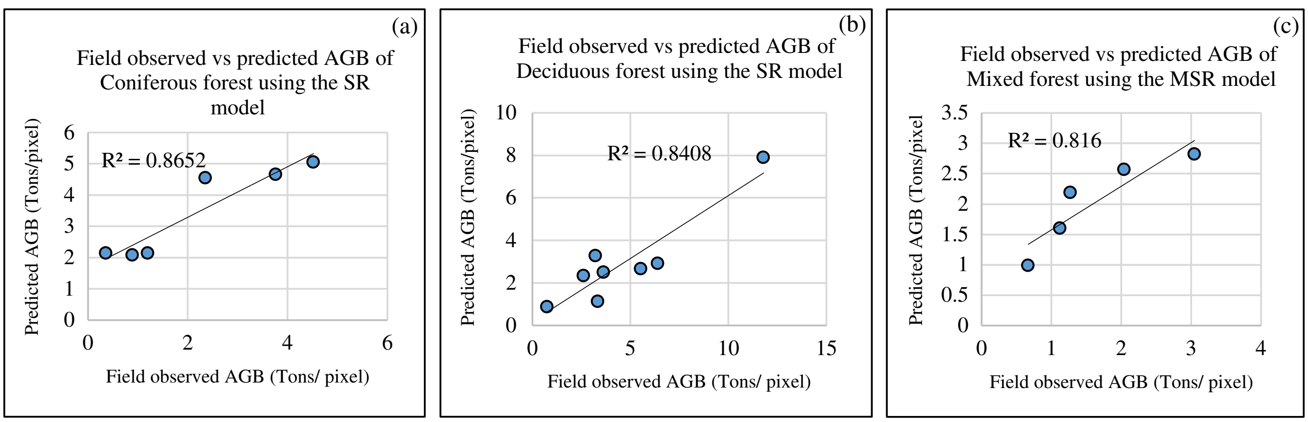

Fig. 6 Validation plot between observed and predicted AGB of coniferous (**a**), deciduous (**b**), and mixed (**c**) forest using vegetation indices

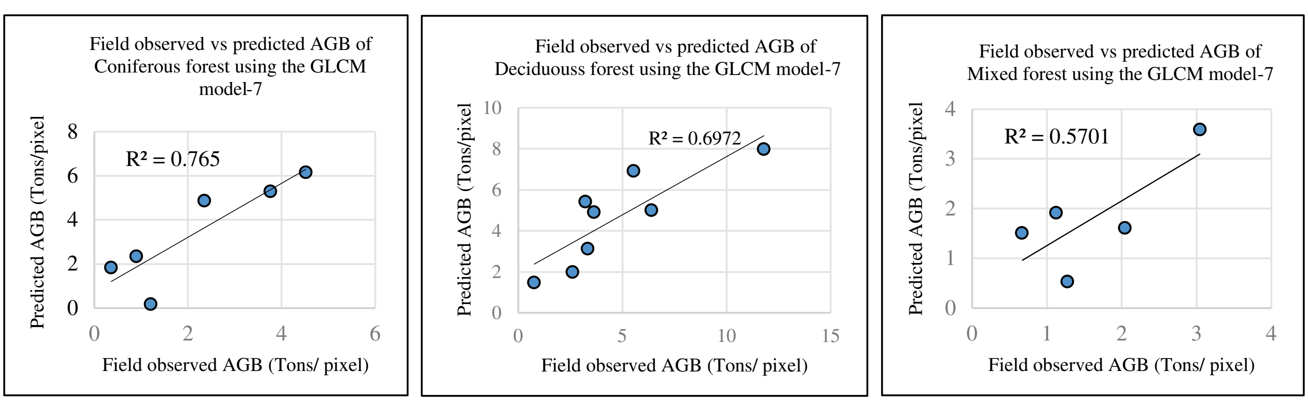

Fig. 7 Validation plot between observed and predicted AGB of coniferous (**a**), deciduous (**b**), and mixed (**c**) forest using GLCM-based models

Table 14 MLR-based combined modeling for coniferous forest

Model	Variable used				Number of variables	Relationship	Model coefficient of determination (r^2)
1	SR	ENT_IR			2	AGB = (0.900518947504234*0.7524*EXP(0.558 4*SR)) + 0.459062580854248*(1.6716*ENT_ IR—6.8163) − 1.58507716896411	0.7479
2	SR	HOM_RED			2	AGB = (0.927435539812124*0.7524*EXP(0.5584 *SR)) + 0.603653709026976*(10.194*HOM_RED − 0.3108) − 2.37985615137042	0.8017
3	SR	ASM_GREEN			2	AGB = (0.993902940489857*0.7524*EXP(0.5584 *SR)) + 0.237232280888233*(6.8828*EXP(− 3.322*ASM_ GREEN)) − 0.925090916245941	0.6951
4	SR	ENT_IR	HOM_RED		3	AGB = (0.816223764075035*0.7524*EXP(0.5584 *SR)) + 0.322871080378063*(1.6716*HOM_RED − 6.8163) + 0.525904860894667*(10.194*ENT_ IR − 0.3108) − 3.01287046960345	0.8307
5	SR	ENT_IR	ASM_GREEN		3	AGB = (0.933436676678785*0.7524*EXP(0.558 4*SR)) + 0.524505729230038*(1.6716*ASM_ GREEN − 6.8163) − 0.150304941066467*(6.8828*EXP(- 3.322*ENT_IR)) − 1.37474112385736	0.7506
6	SR	HOM_RED	ASM_GREEN		3	AGB = (0.838512229643216*0.7524*EXP(0.5584 *SR)) + 0.601272697403676*(10.194*ASM_GREEN − 0.3108) + 0.225654108380577*(6.8828*EXP(− 3.322*H OM_RED)) − 2.96139563179597	0.8106
7	SR	ENT_IR	HOM_RED	ASM_GREEN	4	AGB = (0.820297320671545*0.7524*EXP(0.5584 *SR)) + 0.330865636425123*(1.6716*ASM_GREE N − 6.8163) + 0.524162541451282*(10.194*HOM_ RED − 0.3108) − 0.0173250138195351*(6.8828*EXP (− 3.322*ENT_IR)) − 2.9838956546503	0.8308

Table 15 MLR-based combined modeling for deciduous forest

MODEL	Variable used				Number of variables	Relationship	Model coefficient of determination (r^2)
1	SR	ENT_RED			2	AGB = 0.847644073680865*0.2615*EXP(0.6789 *SR) + 0.804215940553931*0.014*EXP(0.902* ENT_RED) − 1.20380427014967	0.7367
2	SR	ENT_GREEN			2	AGB = 1.09101917779112*0.2615*EXP(0.6789 *SR) + 0.195824526570449*0.0014*EXP(1.257* ENT_GREEN) − 0.341026676494041	0.6866
3	SR	ENT_IR			2	AGB = 1.08414333702256*0.2615*EXP(0.6789 *SR) + 0.35624190867026*0.0037*EXP(0.9324* ENT_IR) − 0.65584228760595	0.6895
4	SR	ENT_RED	ENT_GREEN		3	AGB = 0.921421457720776*0.2615*EXP(0.67 89*SR) − 0.300907742481*0.0014*EXP(1.257* ENT_GREEN) + 1.00389087049466*0.014*EXP(0. 902*ENT_RED) − 1.13955531800184	0.7436
5	SR	ENT_RED	ENT_IR		3	AGB = 0.836792020732083*0.2615*EXP(0.678 9*SR) + 0.790326869665679*0.014*EXP(0.902* ENT_RED) + 0.0540701857301251*0.0037*EXP(0. 9324*ENT_IR) − 1.26575949017129	0.7369
6	SR	ENT_GREEN	ENT_IR		3	AGB = 1.03200167900364*0.2615*EXP(0.6789 *SR) − 0.131125618814277*0.0014*EXP(1.257* ENT_GREEN) + 0.299745975191922*0.0037*EXP (0.9324*ENT_IR) − 0.716369085328599	0.6912
7	SR	ENT_RED	ENT_GREEN	ENT_IR	4	AGB = 0.901864914911025*0.2615*EXP(0.678 9*SR) − 0.31626023959724*0.0014*EXP(1.257* ENT_GREEN) + 0.984231244376142*0.014*EXP (0.902*ENT_ RED) + 0.116195076761434*0.0037*EXP(0.9324* ENT_IR) − 1.2694170570619	0.7442

Table 16 MLR-based combined modeling for mixed forest

MODEL	Variable used				Number of variables	Relationship	Model coefficient of determination (r^2)
1	MSR	ENT_RED			2	AGB = (0.774296358673027*2.4128*MSR^2.8338) + (0.433793896048752*(1.6644*ENT_RED – 6.8199)) – 0.517212125667856	0.78
2	MSR	CON_GREEN			2	AGB = (0.742121701215775*2.4128*MSR^2.8338) + (0.612148654494936*(0.0016*CON_GREEN + 1.556)) – 0.902314039809311	0.86
3	MSR	CON_IR			2	AGB = (0.723404122249626*2.4128*MSR^2.8338) + (0.629628882885919*(0.7872*EXP(0.001*CON_IR))) – 0.788097497406977	0.85
4	MSR	ENT_RED	CON_GREEN		3	AGB = (0.629358242238062*2.4128*MSR^2.8338) + (0.571689969130797*(0.0016*CON_GREEN + 1.556)) + (0.350840410548309*(1.6644*ENT_RED – 6.8199)) – 1.45424388347297	0.90
5	MSR	ENT_RED	CON_IR		3	AGB = (0.710475923449143*2.4128*MSR^2.8338) + (0.0736191328641494*(1.6644*ENT_RED – 6.8199)) + (0.588819137581949*(0.7872*EXP(0.001*CON_IR))) – 0.852088124202343	0.86
6	MSR	CON_GREEN	CON_IR		3	AGB = (0.661096297817618*2.4128*MSR^2.8338) + (0.431974070079122*(0.0016*CON_GREEN + 1.556)) + (0.416592786133718*(0.7872*EXP(0.001*CON_IR))) – 1.25376091189061	0.91
7	MSR	ENT_RED	CON_GREEN	CON_IR	4	AGB = (0.648609247582477*2.4128*MSR^2.8338) + (0.376613117313149*(0.0016*CON_GREEN + 1.556)) + (0.12037360444411*(1.6644*ENT_RED – 6.8199)) + (0.396131933575747*(0.7872*EXP(0.001*CON_IR))) – 1.34826615320316	0.92

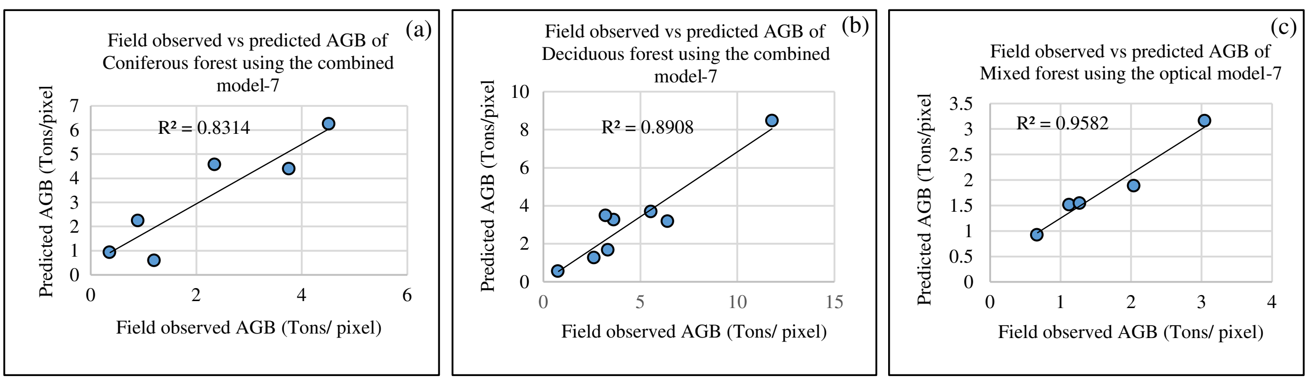

Fig. 8 Validation plot between observed and predicted AGB of coniferous (**a**), deciduous (**b**), and mixed (**c**) forest using combined modeling

Table 17 Detailed model statistics generated from all models for each forest class

Model	Model parameter	Type of forest	Model R^2	Model adjusted R^2	Model standard error (SE) (ton/pixel)	Validation R^2	Validation RMSE (ton/pixel)
Vegetation indices	SR	Deciduous	0.69	0.66	2.17	0.84	2.29
	SR	Coniferous	0.68	0.65	1.08	0.87	1.38
	MSR	Mixed	0.72	0.69	0.81	0.82	0.54
GLCM	ENT_IR, ENT_RED, ENT_GREEN	Deciduous	0.61	0.51	2.61	0.70	1.80
	ENT_IR, HOM_RED, ASM_GREEN	Coniferous	0.59	0.44	1.37	0.77	1.66
	ENT_RED, CON_GREEN, CON_IR	Mixed	0.70	0.55	0.97	0.57	0.69
Combined	SR, ENT_IR, ENT_RED, ENT_GREEN	Deciduous	0.74	0.67	2.16	0.89	1.93
	SR, ENT_IR, HOM_RED, ASM_GREEN	Coniferous	0.83	0.73	0.95	0.83	1.35
	MSR, ENT_RED, CON_GREEN, CON_IR	Mixed	0.92	0.87	0.52	0.96	0.25

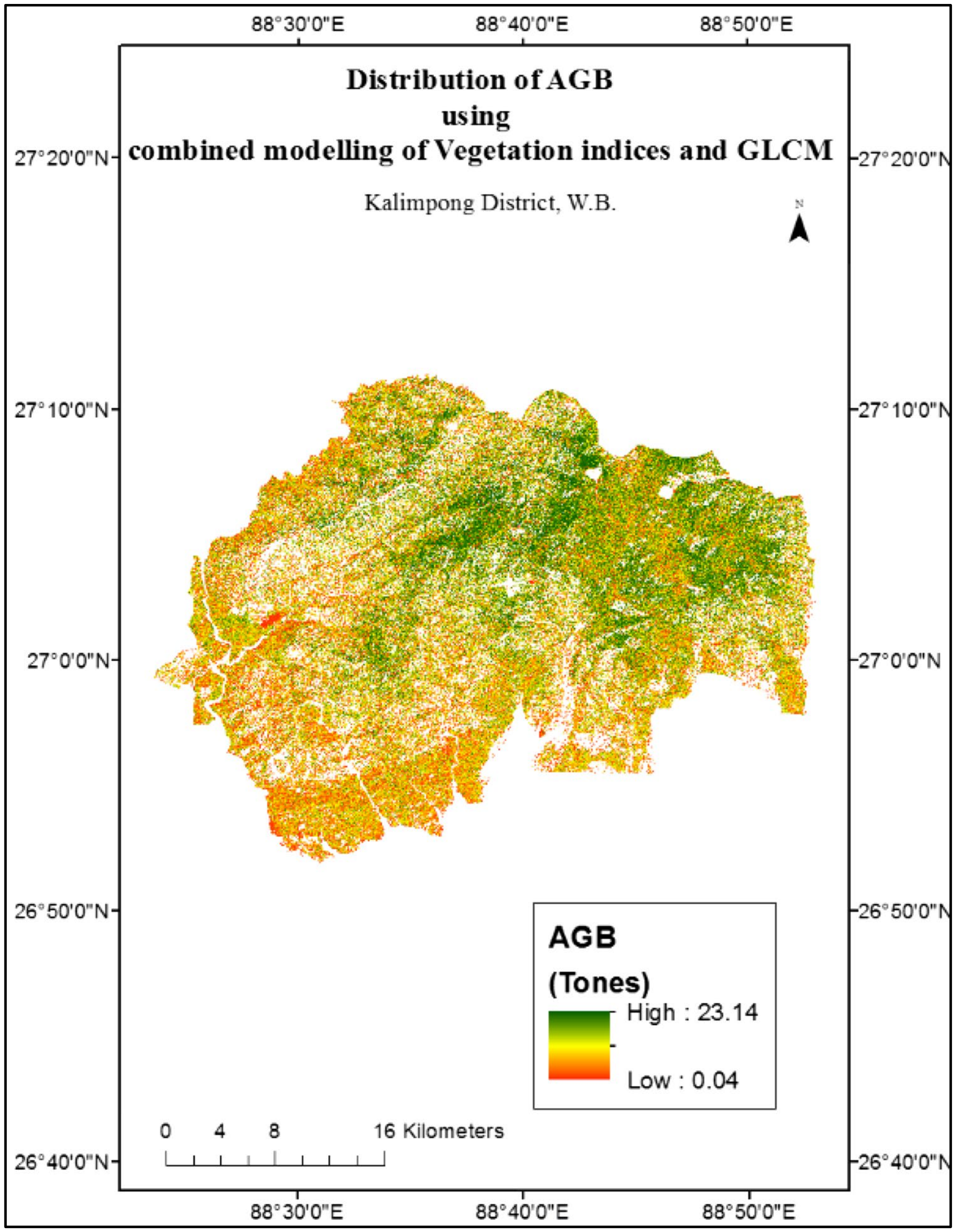

Fig. 9 AGB of Kalimpong forest from combined model

Table 18 ANOVA report of combined model of coniferous forest

	df	*SS*	*MS*	*F*	Significance *F*
Regression	4	30.82359	7.705897	8.591017	0.0007791
Residual	7	6.2788	0.896971		
Total	11	37.10239			

Table 19 ANOVA report of combined model of deciduous forest

	df	*SS*	*MS*	*F*	Significance *F*
Regression	4	177.5391	44.38478	9.457264	0.000826
Residual	13	61.01153	4.693195		
Total	17	238.5507			

an identifier of AGB of Haliyal and Yellapur Forest Divisions, Western Ghats of Karnataka, India. However, Madugundu et al. (2008) did not directly relate to forest AGB and vegetation index (NDVI). Madugundu et al.'s (2008) study was only based on Haliyal and Yellapur Forest's deciduous forest of Western Ghats of Karnataka, India. Pargal et al. (2017), on the other hand, used LISS-IV to investigate the AGB of different forest types in the Yellapur Forest Division, Uttara Kannada District, Western Ghats of Karnataka, India. He used the vegetation index, only NDVI, for his analysis. Pargal et al.'s (2017) AGB model achieved $R^2=0.82$. However, Pargal et al. (2017) cannot generate different AGB models for different forest classes. Attri and Kushwaha (2018) have used LISS-IV data on Barkot Forest Range, Dehradun, India. Attri and Kushwaha (2018) used only NDVI as a vegetation index to identify AGB and got $R^2=0.71$ for his AGB model. Bindu et al. (2020) used kg/pixel-based AGB estimation using LISS-4 generated NDVI. Bindu et al. (2020) achieved an R^2 of 0.71 for his NDVI-based AGB model. However, no studies have used all LISS-4 generated vegetation indices for their AGB modeling. No study has generated an individual AGB model for different forest classes using LISS-4. To date, no study also used LISS-4 generated GLCM-based textures to model forest AGB.

This study correlated high-resolution LISS-4 MSS generated six vegetation indices with AGB. It has been identified that the pure coniferous ($r^2=0.81$) and deciduous forest ($r^2=0.75$) AGB are strongly correlated with SR (Table 7). Due to mixed patches of coniferous and deciduous stands in mixed forest regions, the response of SR is comparatively weaker than the nonlinear vegetation index MSR (Chen 1996). We have found that MSR has a comparatively strong correlation with mixed forest AGB ($r^2=0.84$). Although SR has a strong correlation with pure forest regions, the vegetation index-based model standard error (Table 16) shows that the ability of SR-based model to estimate coniferous forest AGB (SE = 1.08 ton/pixel) is comparatively better than AGB of deciduous forest (SE = 2.17 ton/pixel) due to the presence of varying tree species and so varying spectral responses in deciduous forest. Due to different optical and geometrical surfaces of mixed forest canopies, MSR is a good estimator of mixed forest AGB with SE = 0.81 ton/pixel. These model generated AGB maps have been validated with the field-collected test data sets. The validation of maps also has a strong coefficient of determination (R^2) with field-observed AGB and map generated AGB of deciduous ($R^2=0.84$), coniferous ($R^2=0.87$), and mixed forest ($R^2=0.82$). However, the RMSE of validation is relatively higher in the deciduous forest (2.29 ton/pixel) compared to coniferous (1.38 ton/pixel) and mixed forest (0.54 ton/pixel).

Spectral responses play more essential roles in biomass estimation than textural images when the forest stand structure is relatively simple, but textural images are more important than spectral responses in complex forest stand structures (Lu 2005). Our study has generated 10 GLCM-based texture parameters of 3 different spectral bands of LISS-4 MSS data. These GLCM texture parameters have been correlated with AGB to identify the effect of forest canopy complexity responses among the neighboring pixels. In this study, we have discussed the reasons and justifications for GLCM properties' choice (Table 9). The adjusted R^2 of GLCM models for deciduous (0.51) and mixed forest (0.55) are comparatively better (Table 15) than coniferous forest (0.44). GLCM texture has a better response in complex forest structures with varying tree species. The coniferous forest has fewer tree species than deciduous and mixed forests. The coniferous GLCM model is weaker than the deciduous and mixed forest. Due to higher complexity in tree species variation, the GLCM model of the mixed forest has a higher response than the deciduous forest. These model generated maps of each forest have been validated with the test data. The validation shows that RMSE has reduced in each forest in GLCM models compared to vegetation indices (Table 17). It is seen that the validation R^2 of GLCM models is poor compared to the vegetation index model.

An attempt has been made to combine the models generated by vegetation indices and GLCM-based texture parameters to increase the accuracy of AGB measurement. It has been identified that the combined models have an improvement over individual models (Table 17) in all forest classes. Therefore, the combined models have been chosen to estimate the AGB of each forest class. After generating coniferous, deciduous, and mixed forest AGB maps, the AGB maps have been merged to generate the AGB distribution map of the Kalimpong forest region (Fig. 9). The deciduous forest map shows a validation R^2 of 0.89 with an RMSE of 1.93 ton/pixel. Coniferous forest map validation R^2 is 0.83 with an RMSE of 1.35 ton/pixel. There is a comparatively identifiable improvement in mixed forest with validation R^2 of 0.96 and RMSE of 0.25 ton/pixel. ANOVA report of coniferous, deciduous, and mixed forest is shown in Tables 18, 19, and 20. The equations used to generate the AGB distribution map are given below. The detailed AGB report generated from the AGB distribution map is in Table 21.

Table 20 ANOVA report of combined model of mixed forest

	df	*SS*	*MS*	*F*	Significance *F*
Regression	4	17.5191	4.379776	15.94902	0.0004725
Residual	5	1.373055	0.274611		
Total	9	18.89216			

Table 21 Detailed AGB distribution of Kalimpong forest region

Type of forest	Total AGB (Mt)	Percentage AGB cover (%)	Model R^2	Validation R^2
Deciduous	58.87	56.93	0.74	0.89
Coniferous	36.09	34.91	0.83	0.83
Mixed	8.44	8.16	0.92	0.96
Total (Kalimpong)	**103.40**	**100.00**		

- Coniferous forest: ($r^2 = 0.83$)
  AGB = (0.820297320671545*0.7524*EXP(0.5584*SR)) + 0.330865636425123 * (1.6716 * ASM_GREEN − 6.8163) + 0.524162541451282 *(10.194 * HOM_RED − 0.3108) − 0.0173250138195351 * (6.8828 * EXP(− 3.322*ENT_IR)) − 2.9838956546503.
- Deciduous forest: ($r^2 = 0.74$)
  AGB = 0.901864914911025*0.2615*EXP(0.6789*SR) − 0.31626023959724 * 0.0014 * EXP(1.257 * ENT_GREEN) + 0.984231244376142 * 0.014* EXP(0.902* ENT_RED) + 0.116195076761434 * 0.0037 * EXP(0.9324*ENT_IR) − 1.2694170570619.
- Mixed forest: ($r^2 = 0.92$)

AGB = (0.648609247582477*2.4128*MSR^2.8338) + (0.376613117313149*(0.0016*CON_GREEN + 1.556)) + (0.12037360444411*(1.6644*ENT_RED − 6.8199)) + (0.396131933575747 *(0.7872 * EXP(0.001 *CON_IR))) − 1.34826615320316.

Conclusion

The work envisaged a cost-effective methodology for identifying the AGB of a study area in the Himalayan region. Most of the area in the study area is inaccessible due to rugged terrain and is covered mainly by forest. Due to poor per capita income in the study area, there is much pilferage of forest inventory. To maintain the health of the forest and for regulatory measurement of the forest, it was decided to use LISS-4 data for this work. There are various options available today in identifying AGB using the remote sensing approach, but using low-cost data will reduce the total cost of the analysis for periodic measurement of AGB.

This study suggested that LISS-4 MSS data can estimate the high-resolution AGB distribution of the Himalayan Forest region with adequate accuracy. Various options available for AGB estimation using optical remote sensing data were attempted in work. In this study, six vegetation indices have been used for AGB estimation of different forests of Kalimpong forest regions. Among them, SR gives the highest correlation with AGB of pure deciduous and coniferous forests. In mixed forest regions, due to a mixture of two canopy stands, there is a mixture of foliage angle and optical scattering distribution. Therefore, the nonlinear vegetation index of SR (i.e., MSR) becomes dominant in AGB estimation in mixed forest. It was found that GLCM-based texture parameters of LISS-4 bands have the ability of AGB estimation. Attempts were made to identify the AGB using the GLCM parameters. The results obtained depicted varying accuracy wherein some categories of forest GLCM parameters showed better results, whereas in some types the vegetation indices had better accuracy. An attempt was made to integrate GLCM textures with vegetation indices to identify whether a better accuracy could be obtained in the AGB estimation of the study area. The results obtained have enhanced the AGB model strength for all forest regions, so the integrated model using vegetation indices and the GLCM parameters were selected for the calculation of AGB of the study area.

This study shows AGB storage of deciduous forest has a maximum share over other forest regions of Kalimpong forest. Not only in pure deciduous and coniferous regions, this study has developed an adequately accurate model for mixed forest regions also, where there is a mixture of different canopy cover. The study has also concluded an adequately accurate model with more cost-effectiveness than L band microwave data for AGB modeling.

This model can be used to estimate accurate AGB of different forest regions. Integration of microwave data with LISS-4 can improve the accuracy of AGB monitoring in the future. This model can be beneficial for use in carbon budgeting.

Appendix

Table 22 Plot-wise vegetation index distribution of coniferous forest used to train AGB model

Sl. number	Plot no	Above ground biomass (AGB) [tons/ha]	Above ground biomass (AGB) [tons/pixel]	MSR	NDVI	RDVI	SAVI	SR	TVI
1	2	927.7517	2.319379	0.581127	0.335075	0.38942	0.327667	2.007858	0.913824
2	3	1942.688	4.856719	1.199063	0.56147	0.576612	0.666637	3.560691	1.030277
3	7	2677.199	6.692998	1.152446	0.547917	0.537121	0.646104	3.423966	1.023678
4	8	2903.594	7.258984	1.211049	0.564876	0.567134	0.671649	3.596391	1.031928
5	9	2515.866	6.289666	1.248631	0.575352	0.589885	0.687434	3.709783	1.036992
6	10	1679.119	4.197799	1.196585	0.560762	0.557368	0.665436	3.55334	1.029933
7	18	1439.11	3.597776	0.966498	0.488686	0.514783	0.55765	2.911491	0.994327
8	20	1547.309	3.868272	1.165224	0.551681	0.555569	0.651887	3.461109	1.025515
9	21	2929.369	7.323423	1.233744	0.571239	0.566298	0.681126	3.664603	1.035007
10	22	1686.7	4.21675	1.125022	0.539711	0.567279	0.634109	3.345096	1.019662
11	23	938.0345	2.345086	0.576107	0.332759	0.386869	0.324194	1.997418	0.912556
12	26	1123.687	2.809217	0.702006	0.388251	0.425873	0.407221	2.269315	0.942471

Table 23 Plot-wise vegetation index distribution of deciduous forest used to train AGB model

Sl. number	Plot no	Above ground biomass (AGB) [tons/ha]	Above ground biomass (AGB) [tons/pixel]	MSR	NDVI	RDVI	SAVI	SR	TVI
1	1	326.0192	0.815048	0.469848	0.281596	0.340073	0.247561	1.783949	0.884079
2	5	5383.013	13.45753	1.728696	0.685505	0.693926	0.852439	5.359402	1.088809
3	6	4522.028	11.30507	1.259265	0.578261	0.61894	0.691927	3.74227	1.038393
4	11	465.3523	1.163381	0.461249	0.277273	0.346064	0.241156	1.767297	0.881631
5	12	299.3747	0.748437	0.132296	0.089274	0.173078	0.059555	1.19605	0.767642
6	13	478.2154	1.195539	0.902617	0.466279	0.514374	0.524194	2.747276	0.982995
7	14	1252.013	3.130032	0.875067	0.456267	0.501789	0.509184	2.678276	0.977889
8	15	390.1231	0.975308	0.845384	0.445238	0.492582	0.492668	2.60515	0.972234
9	16	407.9778	1.019944	0.983836	0.494578	0.531717	0.566541	2.957089	0.997285
10	17	1099.099	2.747746	1.344226	0.60066	0.643991	0.725494	4.008264	1.049123
11	19	3109.936	7.77484	1.671958	0.674503	0.681963	0.83595	5.14445	1.083745
12	28	636.4639	1.59116	1.100281	0.532156	0.549379	0.622727	3.274929	1.015951
13	29	1073.342	2.683355	1.169386	0.552899	0.56854	0.653797	3.473262	1.026109
14	33	223.5837	0.558959	0.278977	0.178767	0.253699	0.09359	1.435362	0.823873
15	34	1498.469	3.746174	1.351981	0.602632	0.646235	0.728449	4.033118	1.050063
16	36	746.692	1.86673	1.100281	0.532156	0.549379	0.622727	3.274929	1.015951
17	38	949.3571	2.373393	1.128369	0.540722	0.587839	0.635714	3.354661	1.020158
18	39	443.6311	1.109078	0.396143	0.243617	0.303519	0.190668	1.644163	0.862332

Table 24 Plot-wise vegetation index distribution of mixed forest used to train AGB model

Sl. number	Plot no	Above ground biomass (AGB) [tons/ha]	Above ground biomass (AGB) [tons/pixel]	MSR	NDVI	RDVI	SAVI	SR	TVI
1	4	985.2877	2.463219	1.059282	0.519312	0.56459	0.603633	3.160703	1.00961
2	24	780.4696	1.951174	0.929733	0.475926	0.503459	0.53854	2.816255	0.98789
3	25	1148.409	2.871022	1.097041	0.531156	0.549379	0.622727	3.265811	1.015459
4	27	1109.217	2.773043	1.099185	0.531818	0.559545	0.622285	3.271843	1.015784
5	30	492.1385	1.230346	0.841181	0.443656	0.485196	0.490271	2.594898	0.97142
6	31	320.1169	0.800292	0.698578	0.38681	0.433231	0.40513	2.261632	0.941706
7	43	1743.402	4.358506	1.237287	0.572222	0.6	0.68282	3.675322	1.035482
8	48	2078.953	5.197383	1.30308	0.562615	0.587248	0.663333	3.572631	1.030832
9	49	1687.798	4.219496	0.936894	0.47844	0.49482	0.54222	2.83465	0.989161
10	54	642.2481	1.60562	0.901255	0.465789	0.497738	0.52338	2.743839	0.982746

Table 25 Plot-wise GLCM of green band distribution of coniferous forest used to train AGB model

Sl. no	Above ground biomass (AGB) [tons/ha]	Above ground biomass (AGB) [tons/pixel]	ASM **GREEN**	CON **GREEN**	COR **GREEN**	DIS **GREEN**	ENG **GREEN**	ENT **GREEN**	HOM **GREEN**	MAX **GREEN**	MEAN **GREEN**	VAR **GREEN**
1	927.7517	2.319379	0.296007	571.6667	0.761001	25.75	0.544065	4.898074	0.479838	0.416667	43.625	1195.958
2	1942.688	4.856719	0.123264	719.5	0.758307	31	0.35109	5.955402	0.271764	0.166667	48.33333	1488.458
3	2677.199	6.692998	0.084201	672.5	0.785052	29.25	0.290175	6.536474	0.239677	0.083333	48.04167	1564.333
4	2903.594	7.258984	0.092014	317.25	0.932684	20.66667	0.303338	6.384424	0.210063	0.083333	65.75	2356.417
5	2515.866	6.289666	0.133681	205.375	0.90246	16.95833	0.365624	5.801033	0.293017	0.166667	43.8125	1052.771
6	1679.119	4.197799	0.115646	400.619	0.938142	23.47619	0.340068	6.093194	0.313665	0.142857	78.11905	3238.214
7	1439.11	3.597776	0.203125	215.7083	0.914834	17.29167	0.450694	5.029068	0.290449	0.208333	48.35417	1266.396
8	1547.309	3.868272	0.124132	651.4583	0.924123	30.29167	0.352324	5.961273	0.30386	0.145833	88.64584	4292.854
9	2929.369	7.323423	0.088154	713.9394	0.867831	31.87879	0.296908	6.415187	0.090475	0.090909	69.0303	2700.848
10	1686.7	4.21675	0.085069	768.8333	0.844095	32.33333	0.291667	6.535909	0.201772	0.083333	64.66666	2465.708
11	938.0345	2.345086	0.077562	759	0.878251	33.10526	0.2785	6.709353	0.12855	0.078947	73.28947	3117.079
12	1123.687	2.809217	0.269097	135.5833	0.945287	12.66667	0.609531	4.424138	0.621555	0.5	48.58333	1239.042

Table 26 Plot-wise GLCM of red band distribution of coniferous forest used to train AGB model

Sl. no	Above ground biomass (AGB) [tons/ha]	Above ground biomass (AGB) [tons/pixel]	ASM **RED**	CON **RED**	COR **RED**	DIS **RED**	ENG **RED**	ENT **RED**	HOM **RED**	MAX **RED**	MEAN **RED**	VAR **RED**
1	927.7517	2.319379	0.196181	632	0.307081	27	0.442923	4.79205	0.392568	0.145833	18.75	456.0417
2	1942.688	4.856719	0.196181	632	0.307081	27	0.442923	4.79205	0.392568	0.145833	18.75	456.0417
3	2677.199	6.692998	0.205729	7054.792	0.453659	82.79166	0.453574	5.403776	0.506612	0.333333	68.5625	6456.396
4	2903.594	7.258984	0.283854	372.2917	0.314643	17.625	0.53278	4.376338	0.742807	0.333333	12.9375	271.6042
5	2515.866	6.289666	0.212674	2309.375	0.337093	51.04167	0.461165	4.911024	0.485104	0.25	36.5625	1741.854
6	1679.119	4.197799	0.211806	679.0833	0.435821	25.5	0.460223	4.903945	0.576782	0.25	20.125	601.8333
7	1439.11	3.597776	0.223958	665.25	0.475044	28.5	0.473242	4.668136	0.471028	0.1875	24.79167	633.625
8	1547.309	3.868272	0.141493	3130.333	0.412135	53.91667	0.376156	5.684944	0.379922	0.125	43.16667	2662.458
9	2929.369	7.323423	0.240451	988.875	0.268876	31.375	0.490358	4.840312	0.57156	0.333333	21.85417	676.2708
10	1686.7	4.21675	0.194444	1254.792	0.310412	36.79167	0.440959	4.93347	0.368499	0.1875	26.10417	909.8125
11	938.0345	2.345086	0.249307	3043.368	0.22629	52.63158	0.499307	4.694875	0.431626	0.315789	33.47368	1966.737
12	1123.687	2.809217	0.263889	2082.625	0.102881	37.95833	0.513701	4.396567	0.518525	0.25	22.39583	1160.729

Table 27 Plot-wise GLCM of IR band distribution of coniferous forest used to train AGB model

Sl. no	Above ground biomass (AGB) [tons/ha]	Above ground biomass (AGB) [tons/pixel]	ASM **IR**	CON **IR**	COR **IR**	DIS **IR**	ENG **IR**	ENT **IR**	HOM **IR**	MAX **IR**	MEAN **IR**	VAR **IR**
1	927.7517	2.319379	0.125868	3312	0.67757	63.5	0.354779	6.333741	0.30273	0.25	83.875	5136
2	1942.688	4.856719	0.074653	2965.875	0.837883	63.54167	0.273227	6.832364	0.092225	0.083333	124.2292	9147.313
3	2677.199	6.692998	0.049479	1349.25	0.808273	42.5	0.222439	7.482472	0.094755	0.041667	73.33334	3518.667
4	2903.594	7.258984	0.045139	1253.542	0.946717	42.375	0.212459	7.626877	0.037375	0.041667	149.2292	11,763.02
5	2515.866	6.289666	0.063368	491.8333	0.877501	26	0.25173	7.056334	0.202969	0.0625	59.79167	2007.5
6	1679.119	4.197799	0.061728	3092.444	0.906698	66.55556	0.248452	7.013005	0.029975	0.055556	174.2778	16,572.28
7	1439.11	3.597776	0.057292	1000.667	0.872687	38.16667	0.239357	7.222542	0.14329	0.041667	83.58334	3929.958
8	1547.309	3.868272	0.138889	1922.792	0.946599	50.375	0.372678	6.066167	0.255664	0.1875	184.3958	18,003.44
9	2929.369	7.323423	0.053819	654.1667	0.969203	29.75	0.23199	7.338066	0.146901	0.041667	143.4167	10,620.58
10	1686.7	4.21675	0.063368	1614.417	0.774992	46	0.25173	7.056334	0.177074	0.0625	74.20834	3587.458
11	938.0345	2.345086	0.059557	2145.474	0.849643	55.15789	0.244043	7.092765	0.09322	0.052632	109.0526	7134.579
12	1123.687	2.809217	0.197049	128.2083	0.917278	12.04167	0.443902	5.178033	0.572439	0.25	38.02083	774.9375

Table 28 Plot-wise GLCM of green band distribution of deciduous forest used to train AGB model

Sl. no	Above ground biomass (AGB) [tons/ha]	Above ground biomass (AGB) [tons/pixel]	ASM GREEN	CON GREEN	COR GREEN	DIS GREEN	ENG GREEN	ENT GREEN	HOM GREEN	MAX GREEN	MEAN GREEN	VAR GREEN
1	326.0192	0.815048	0.177951	339.75	0.931462	19.25	0.421843	5.387743	0.416201	0.25	67.66666	2478.542
2	5383.013	13.45753	0.083333	529.7083	0.946591	28.125	0.288675	6.623117	0.108553	0.083333	97.22916	4958.938
3	4522.028	11.30507	0.117188	352.25	0.973431	21.41667	0.342327	6.020244	0.246288	0.125	113.6667	6628.958
4	465.3523	1.163381	0.168962	1878	0.763481	49.15152	0.41105	5.39166	0.196659	0.181818	79.72727	3970.091
5	299.3747	0.748437	0.18316	100.625	0.996641	12.125	0.427972	5.127248	0.297334	0.1875	172.8542	14,979.65
6	478.2154	1.195539	0.183673	327.1429	0.983437	22.28572	0.428571	4.88203	0.055864	0.142857	139.7143	9875.571
7	1252.013	3.130032	0.078993	556.7083	0.968704	27.20833	0.281057	6.6738	0.242364	0.083333	130.9792	8894.354
8	390.1231	0.975308	0.179688	278.5	0.988875	20	0.423896	4.938673	0.178081	0.125	157.625	12,517
8	407.9778	1.019944	0.142857	733.8571	0.967387	33	0.377964	5.278115	0.029187	0.071429	148.0714	11,250.93
10	1099.099	2.747746	0.111979	526.5	0.979361	24.66667	0.334633	6.078006	0.368436	0.125	157.875	12,754.96
11	3109.936	7.77484	0.082465	737.9167	0.911709	31.5	0.287168	6.663272	0.235227	0.104167	87.16666	4178.875
12	636.4639	1.59116	0.16059	223.25	0.883314	16.25	0.400737	5.406198	0.281027	0.145833	41.125	956.625
13	1073.342	2.683355	0.099881	1895.379	0.901295	51.10345	0.31604	6.17267	0.11392	0.103448	132.3793	9601.275
14	223.5837	0.558959	0.154514	274.0833	0.940697	18.33333	0.393083	5.337059	0.369208	0.166667	66.33334	2310.875
15	1498.469	3.746174	0.091111	866.1334	0.941214	36	0.301846	6.294087	0.091887	0.066667	117.9333	7366.8
16	746.692	1.86673	0.099826	597.8333	0.94044	28.33333	0.315953	6.232375	0.237119	0.125	97.29166	5018.75
17	949.3571	2.373393	0.102079	1358.783	0.92712	45.04348	0.319499	6.029894	0.013895	0.086957	132.6956	9322.087
18	443.6311	1.109078	0.123457	1448.667	0.922656	46.22222	0.351364	5.626711	0.014718	0.111111	132.7778	9365.111

Table 29 Plot-wise GLCM of red band distribution of deciduous forest used to train AGB model

Sl. no	Above ground biomass (AGB) [tons/ha]	Above ground biomass (AGB) [tons/pixel]	ASM RED	CON RED	COR RED	DIS RED	ENG RED	ENT RED	HOM RED	MAX RED	MEAN RED	VAR RED
1	326.0192	0.815048	0.394097	4282.208	0.202661	70.375	0.627772	4.203821	0.58739	0.416667	43.47917	2685.313
2	5383.013	13.45753	0.0925	6479.9	0.461158	93.5	0.304138	6.476667	0.104696	0.1	81.3	6012.8
3	4522.028	11.30507	0.094618	3806.583	0.722929	71.5	0.3076	6.442751	0.149207	0.083333	95.75	6869.333
4	465.3523	1.163381	0.339761	6932.485	0.274025	89.21212	0.58289	4.12529	0.547833	0.363636	61.87879	4774.606
5	299.3747	0.748437	0.146701	225.375	0.996143	12.95833	0.383016	5.541849	0.523923	0.125	241.3125	29,212.56
6	478.2154	1.195539	0.180556	1862.75	0.955836	50.25	0.424918	5.113654	0.194496	0.166667	201.375	21,088.79
7	1252.013	3.130032	0.09375	4244.667	0.826706	76	0.306186	6.261256	0.169851	0.0625	143.4167	12,247
8	390.1231	0.975308	0.164063	5500.375	0.862266	87.625	0.405046	5.11196	0.130689	0.125	190.1875	19,967.44
8	407.9778	1.019944	0.142857	8733.571	0.688206	119.5714	0.377964	5.278115	0.002527	0.071429	144.9286	14,005.36
10	1099.099	2.747746	0.118056	4214.667	0.895936	66.16666	0.343592	6.378656	0.319086	0.208333	190.0833	20,250.29
11	3109.936	7.77484	0.091146	5271.417	0.433029	81.33334	0.301904	6.399147	0.234514	0.083333	66.41666	4648.75
12	636.4639	1.59116	0.201389	819.9167	0.256368	27.58333	0.448764	4.861549	0.536972	0.166667	18.25	551.2917
13	1073.342	2.683355	0.095125	10,690.34	0.697565	122.3448	0.308423	6.208756	0.167819	0.068966	161.931	17,673.79
14	223.5837	0.558959	0.463542	860.8333	0.059199	24.66667	0.680839	4.022144	0.844026	0.583333	13.5	457.5
15	1498.469	3.746174	0.091049	6044.5	0.715965	94.94444	0.301744	6.329297	0.059915	0.083333	123.6389	10,640.42
16	746.692	1.86673	0.148438	2212.583	0.643596	55.58333	0.385276	5.543525	0.233625	0.145833	63	3104.042
17	949.3571	2.373393	0.12963	9845	0.783853	102.7778	0.360041	5.549695	0.157914	0.111111	195.0556	22,773.83
18	443.6311	1.109078	0.12963	9845	0.783853	102.7778	0.360041	5.549695	0.157914	0.111111	195.0556	22,773.83

Table 30 Plot-wise GLCM of IR band distribution of deciduous forest used to train AGB model

Sl. no	Above ground biomass (AGB) [tons/ha]	Above ground biomass (AGB) [tons/pixel]	ASM_IR	CON_IR	COR_IR	DIS_IR	ENG_IR	ENT_IR	HOM_IR	MAX_IR	MEAN_IR	VAR_IR
1	326.0192	0.815048	0.065972	552.25	0.975473	27.16667	0.256851	7.099373	0.121024	0.083333	148.4583	11,257.96
2	5383.013	13.45753	0.047743	923.9583	0.927881	35.20833	0.218502	7.540234	0.0885	0.041667	109.2708	6405.771
3	4522.028	11.30507	0.055309	288.2222	0.988269	18.97778	0.235178	7.274453	0.171682	0.044444	155.9778	12,284.91
4	465.3523	1.163381	0.12066	1530.708	0.897123	44.375	0.347361	6.248408	0.326076	0.208333	116.4375	7439.521
5	299.3747	0.748437	0.069444	477.0833	0.927209	26.08333	0.263523	6.890126	0.13596	0.0625	78.75	3277.083
6	478.2154	1.195539	0.065744	496.9412	0.872475	26.35294	0.256406	6.889627	0.11209	0.058824	59	1948.412
7	1252.013	3.130032	0.0625	314.6667	0.958674	20.91667	0.25	7.164779	0.168696	0.083333	85.54166	3807.083
8	390.1231	0.975308	0.086667	1569.867	0.915645	47.73333	0.294392	6.386507	0.079394	0.066667	132.1333	9305.134
8	407.9778	1.019944	0.090909	903.7273	0.933199	35.18182	0.301511	6.182085	0.038958	0.045455	111.9545	6764.318
10	1099.099	2.747746	0.049479	1148.792	0.967355	36.29167	0.222439	7.482472	0.167416	0.041667	184.3542	17,595.35
11	3109.936	7.77484	0.046007	1674.833	0.946336	47.08333	0.214492	7.597996	0.125377	0.041667	172.0833	15,604.79
12	636.4639	1.59116	0.072917	450.875	0.884535	22.375	0.270031	6.854166	0.252247	0.083333	59.14583	1952.438
13	1073.342	2.683355	0.0625	2555.063	0.923989	60.0625	0.25	6.931472	0.057364	0.03125	176.5313	16,807.09
14	223.5837	0.558959	0.154321	442.6667	0.980704	24.44445	0.392837	5.337523	0.226197	0.166667	150.3333	11,470.67
15	1498.469	3.746174	0.084775	271.1765	0.994913	18	0.291162	6.441121	0.206579	0.058824	230.2941	26,653.53
16	746.692	1.86673	0.050347	1162.75	0.966374	37.83333	0.224382	7.453591	0.164904	0.041667	182.9167	17,289.25
17	949.3571	2.373393	0.098299	1345.304	0.939863	41.82609	0.313526	6.090168	0.155367	0.086957	145.8696	11,185.26
18	443.6311	1.109078	0.098299	1345.304	0.939863	41.82609	0.313526	6.090168	0.155367	0.086957	145.8696	11,185.26

Table 31 Plot-wise GLCM of green band distribution of mixed forest used to train AGB model

Sl. number	Above ground biomass (AGB) [tons/ha]	Above ground biomass (AGB) [tons/pixel]	ASM **GREEN**	CON **GREEN**	COR **GREEN**	DIS **GREEN**	ENG **GREEN**	ENT **GREEN**	HOM **GREEN**	MAX **GREEN**	MEAN **GREEN**	VAR **GREEN**
1	985.2877	2.463219	0.069444	842.375	0.821299	32.04167	0.263523	6.93373	0.128387	0.083333	62.14583	2356.938
2	780.4696	1.951174	0.09375	688.5	0.908774	30.16667	0.306186	6.48579	0.200193	0.125	83.33334	3773.583
3	1148.409	2.871022	0.198785	303.625	0.958146	19.29167	0.445853	5.539895	0.331108	0.291667	83.60416	3627.188
4	1109.217	2.773043	0.12066	275.75	0.962792	19.25	0.347361	5.825155	0.174423	0.104167	84.5	3705.542
5	492.1385	1.230346	0.121528	285.875	0.987134	18.79167	0.348608	5.930716	0.312106	0.125	148.2708	11,109.4
6	320.1169	0.800292	0.136285	384.8333	0.982963	21.33333	0.369168	5.915247	0.263731	0.166667	149.2917	11,294.29
7	1743.402	4.358506	0.09809	392.5833	0.979635	23.58333	0.313194	6.424579	0.164323	0.125	137.5417	9638.667
8	2078.953	5.197383	0.061728	2025.056	0.761016	54.5	0.248452	7.013005	0.0246	0.055556	81.47222	4236.806
9	1687.798	4.219496	0.098619	1614.821	0.804233	43.64103	0.314037	6.349261	0.234329	0.153846	83.20513	4124.333
10	642.2481	1.60562	0.111979	438.2917	0.939404	25.79167	0.334633	6.027887	0.148923	0.104167	82.8125	3616.521

Table 32 Plot-wise GLCM of red band distribution of mixed forest used to train AGB model

Sl. number	(AGB) [tons/ha]	Above ground biomass (AGB) [tons/pixel]	ASM **RED**	CON **RED**	COR **RED**	DIS **RED**	ENG **RED**	ENT **RED**	HOM **RED**	MAX **RED**	MEAN **RED**	VAR **RED**
1	985.2877	2.463219	0.221354	2546.458	0.274969	49.04167	0.470483	5.175611	0.567226	0.333333	32.52083	1756.104
2	780.4696	1.951174	0.139757	1945.667	0.371132	48.58333	0.373841	5.514541	0.386993	0.125	37	1546.958
3	1148.409	2.871022	0.126736	2700.667	0.472869	53.75	0.356	5.854036	0.284074	0.125	44.45833	2561.667
4	1109.217	2.773043	0.161458	1877.125	0.318287	39.20833	0.401819	5.328407	0.426411	0.166667	29.89583	1376.771
5	492.1385	1.230346	0.270062	65.33334	0.99892	7.555555	0.519675	4.865369	0.703899	0.388889	245.7778	30,235.5
6	320.1169	0.800292	0.122396	1444	0.969141	39.66667	0.349851	5.929405	0.337925	0.166667	213.5417	23,396.38
7	1743.402	4.358506	0.074653	6972.708	0.565702	101.125	0.273227	6.78876	0.087122	0.0625	101.1458	8027.563
8	2078.953	5.197383	0.106667	1910.5	0.514257	49.5	0.326599	6.215801	0.246378	0.111111	103.2444	10,309.42
9	1687.798	4.219496	0.114398	10,186.62	0.379383	113.5897	0.338228	6.064892	0.238984	0.102564	87.8718	8206.846
10	642.2481	1.60562	0.131944	3259.083	0.294202	61	0.363242	5.741395	0.278829	0.125	45	2308.792

Table 33 Plot-wise GLCM of IR band distribution of mixed forest used to train AGB model

Sl. number	Above ground biomass (AGB) [tons/ha]	Above ground biomass (AGB) [tons/pixel]	ASM IR	CON IR	COR IR	DIS IR	ENG IR	ENT IR	HOM IR	MAX IR	MEAN IR	VAR IR
1	985.288	2.463219	0.04774	695.0417	0.979381	31.875	0.218502	7.54023	0.071819	0.041667	181.729	16,854.2
2	780.47	1.951174	0.05295	1371.867	0.910812	33.58333	0.230112	7.36695	0.076547	0.041667	92.2917	4726
3	1148.41	2.871022	0.04642	1298.489	0.939076	41.95556	0.215452	7.55171	0.092923	0.044444	142.311	10,656.6
4	1109.22	2.773043	0.04688	787.7083	0.819917	55.20833	0.216506	7.56912	0.021712	0.041667	99.4792	5807.4
5	492.139	1.230346	0.08929	441.3571	0.986451	24.07143	0.298807	6.31784	0.165138	0.071429	179.393	16,287.5
6	320.117	0.800292	0.15385	579.5385	0.984591	27.84615	0.392232	5.1299	0.205963	0.076923	192.539	18,804.7
7	1743.4	4.358506	0.0434	1373.208	0.963327	43.29167	0.208333	7.07926	0.04213	0.041667	189.896	18,722.6
8	2078.95	5.197383	0.0434	1488.542	0.846883	42.04167	0.208333	7.68464	0.067944	0.041667	91.8542	4860.81
9	1687.8	4.219496	0.04444	1655.244	0.865047	47.42222	0.210819	7.61333	0.082028	0.022222	103.267	6132.69
10	642.248	1.60562	0.04514	1247.083	0.935146	41.41667	0.212459	7.62688	0.057065	0.041667	134.25	9614.58

Acknowledgements The researchers are thankful to the Department of Science and Technology, New Delhi for providing the opportunity to work in this area.

Funding The researchers received funding for this project from the Department of Science and Technology, New Delhi.

Declarations

Conflict of interest The authors declare no competing interests.

References

Ali A, Ullah S, Bushra S, Ahmad N, Ali A, Khan M (2018) Quantifying forest carbon stocks by integrating satellite images and forest inventory data. Austrian J for Sci 135(2):93–118

Askar NN, Phairuang W, Wicaksono P, Sayektiningsih T (2018) Estimating aboveground biomass on private forest using Sentinel-2 Imagery. J Sens 2018:11. https://doi.org/10.1155/2018/6745629

Attri P, Kushwaha S (2018) Estimation of biomass and carbon pool in Barkot Forest Range, UK using geospatial tools. ISPRS Ann Photogramm Remote Sens Spatial Inf Sci 4(5):121–128. https://doi.org/10.5194/isprs-annals-IV-5-121-2018

Avitabile V, Baccini A, Friedl M, Schmullius C (2012) Capabilities and limitations of Landsat and land cover data for aboveground woody biomass estimation of Uganda. Remote Sens Environ 117:366–380

Barrachina M, Cristóbal J, Tulla A (2015) Estimating above-ground biomass on mountain meadows and pastures through remote sensing. Int J Appl Earth Obs Geoinf 38:184–192

Bindu G, Rajan P, Jishnu ES, Joseph KA (2020) Carbon stock assessment of mangroves using remote sensing and geographic information system. Egypt J Remote Sens 23(1):1–9

Blomberg E, Ferro-Famil L, Ulander L (2018) Forest biomass retrieval from L-band SAR using tomographic ground backscatter removal. IEEE Geosci Remote Sens Lett 15(7):1030–1034

Brown S (1997) Estimating biomass and biomass change of tropical forests: a primer. A Forest Resources Assessment publication, Rome

Brown S, Lugo A (1992) Above ground biomass estimates for tropical moist forests of the Brazilian Amazon. Interciencia Interciencia 17(1):8–18

Chen J (1996) Evaluation of vegetation indices and a modified simple ratio for boreal applications. Can J Remote Sens 22(3):229–242

Chen J, Chilar J (1996) Retrieving leaf area index of boreal conifer forests using Landsat TM images. Remote Sens Environ 55(2):153–162

Das S, Singh T (2016) Forest type, diversity and biomass estimation in tropical forests of Western Ghat of Maharashtra using geospatial techniques. Small-Scale for 15:517–532

Du H, Zhou G, Ge H, Fan W, Xu X, Fan W, Shi Y (2012) Satellite-based carbon stock estimation for bamboo forest with a non-linear partial least square regression technique. Int J Remote Sens 33(6):1917–1933

Dube T, Mutanga O, Shoko C, Adelabu S, Bangira T (2016) Remote sensing of aboveground forest biomass: a review. Trop Ecol 57(2):125–132

Foody G, Boyd D, Cutler M (2003) Predictive relations of tropical forest biomass from Landsat TM data and their transferability between regions. Remote Sens Environ 85(4):463–474

Fuchs H, Magdon P, Kleinn C, Flessa H (2009) Estimating above-ground carbon in a catchment of the Siberian forest tundra: combining satellite imagery and field inventory. Remote Sens Environ 113(3):518–531

Gascón L, Ceccherini G, Haro F, Avitabile V, Eva H (2019) The potential of high resolution (5 m) RapidEye optical data to estimate

above ground biomass at the national level over Tanzania. Forests 10(2):107
Günlü A, Ercanli I (2020) Artificial neural network models by ALOS PALSAR data for aboveground stand carbon predictions of pure beech stands: a case study from northern of Turkey. Geocarto in 35(1):17–28
Günlü A, Ercanli I, Başkent E, Çakır G (2014) Estimating aboveground biomass using Landsat TM imagery: a case study of Anatolian Crimean pine forests in Turkey. Ann for Res 57(2):289–298
Hall R, Skakun R, Arsenault E, Case B (2006) Modeling forest stand structure attributes using Landsat ETM+ data: application to mapping of aboveground biomass and stand volume. For Ecol Manage 225(1–3):378–390
Haralick R, Shanmugam K, Dinstein I (1973) Textural features for image classification. IEEE Trans Syst Man Cybern Syst SMC 3(6):610–621
Huete A (1988) A soil-adjusted vegetation index (SAVI). Remote Sens Environ 25(3):295–309
Jackson R, Slater P, Pinter P (1983) Discrimination of growth and water stress in wheat by various vegetation indices through clear and turbid atmospheres. Remote Sens Environ 13(3):187–208
Kayitakire F, Hamel C, Defourny P (2006) Retrieving forest structure variables based on image texture analysis and IKONOS-2 imagery. Remote Sens Environ 102(3–4):390–401
Keleş S, Günlü A, Ercanli I (2021) Estimating aboveground stand carbon by combining Sentinel-1 and Sentinel-2 satellite data: a case study from Turkey. Forest Resources Resilience and Conflicts 117–126. https://doi.org/10.1016/B978-0-12-822931-6.00008-3
Kumar P, Sharma L, Pandey P, Sinha S, Nathawat M (2013) Geospatial strategy for tropical forest-wildlife reserve biomass estimation. IEEE J Sel Top Appl Earth Obs Remote Sens 6(2):917–923
Kurvonen L, Pulliainen J, Hallikainen M (1999) Retrieval of biomass in boreal forests from multitemporal ERS-1 and JERS-1 SAR images. IEEE Trans Geosci Remote Sens 37(1):198–205
Li B, Wang W, Bai L, Chen N, Wang W (2018) Estimation of aboveground vegetation biomass based on Landsat-8 OLI satellite images in the Guanzhong Basin. China Int J Remote Sens 40(10):3927–3947
Lu D (2005) Aboveground biomass estimation using Landsat TM data in the Brazilian Amazon. I Int J Remote Sens 26:2509–2525
Lu D, Batistella M (2005) Exploring TM image texture and its relationships with biomass estimation in Rondônia. Brazilian Amazon Acta Amazonica 35(2):249–257
Lu D, Batistella M, Moran E (2005) (a)) Satellite estimation of aboveground biomass and impacts of forest stand structure. Photogramm Eng Remote Sens 71(8):967–974
Lu D, Chen Q, Wang G, Liu L, Li G, Moran E (2016) A survey of remote sensing-based aboveground biomass estimation methods in forest ecosystems. Int J Digital Earth 9(1):63–105
Luckman A, Baker J, Kuplich T, Yanasse C, Frery A (1997) A study of the relationship between radar backscatter and regenerating forest biomass for space borne SAR instrument. Remote Sens Environ 60(1):1–13
Madugundu R, Nizalapur V, Jha C (2008) Estimation of LAI and above-ground biomass in deciduous forests: Western Ghats of Karnataka, India. Int J Appl Earth Obs Geoinf 10(2):211–219
Mareya H, Tagwireyi P, Ndaimani H, Gara T, Gwenzi D (2018) Estimating tree crown area and aboveground biomass in Miombo Woodlands from high-resolution RGB-only imagery. IEEE J Sel Top Appl Earth Obs Remote Sens 11(3):868–875
Mayamanikandan T, Jha C, Das I, Amminedu E, Reddy C (2017) Forest biomass estimation in tropical deciduous forests of western ghats using remote sensing data and GIS. In: 3rd International Conference on Environmental Management. Centre for Environment, JNTU, Hyderabad. https://www.researchgate.net/publication/329012038_Forest_Biomass_Estimation_in_Tropical_Deciduous_Forests_of_Western_Ghats_using_Remote_sensing_data_and_GIS
Nandy S, Singh R, Ghosh S, Watham T, Singh Kushwaha S, Kumar A, Dadhwal V (2017) Neural network-based modelling for forest. Carbon Manage. https://doi.org/10.1080/17583004.2017.1357402
Nesha M, Hussin Y, Leeuwen L, Sulistioadi Y (2020) Modeling and mapping aboveground biomass of the restored mangroves using ALOS-2 PALSAR-2 in East Kalimantan, Indonesia. Int J Appl Earth Observ Geoinfo 91:102158
Obeyed M, Mustafa Y, Akrawee Z (2018) Estimating and Mapping Aboveground Biomass of Natural Quercus Aegilops Using WorldView-3 Imagery. International Conference on Advanced Science and Engineering (ICOASE), Kurdistan Region, Iraq. https://ieeexplore.ieee.org/document/8548859
Pandit S, Tsuyuki S, Dube T (2018) Estimating above-ground biomass in sub-tropical buffer zone community forests, Nepal, using Sentinel 2 data. Remote Sens 10(4):601
Pargal S, Fararoda R, Rajashekar G, Balachandran N, Réjou-Méchain M, Barbier N, Jha CS, Pélissier R, Dadhwal VK, Couteron P (2017) Inverting aboveground biomass-canopy texture relationships in a landscape of forest mosaic in the western Ghats of India using very high resolution Cartosat imagery. Remote Sens 9:228. https://doi.org/10.3390/rs9030228
Parresol B (1999) Assessing tree and stand biomass: a review with examples and critical comparisons. For Sci 45(4):573–593
Pearson R, Miller L (1972) Remote mapping of standing crop biomass for estimation of the productivity of the shortgrass prairie. In: Proceedings of the 8th International Symposium on Remote Sensing of the Environment. Colorado State University, Pawnee National Grasslands, Colorado. https://eurekamag.com/research/000/179/000179997.php
Perry C, Lautenschlager L (1984) Functional equivalence of spectral vegetation indices. Remote Sens Environ 14(1–3):169–182
Phua M, Saito H (2003) Estimation of biomass of a mountainous tropical forest using Landsat TM data. Can J Remote Sens 29(4):429–440
Roujean J, Breon F (1995) Estimating PAR Absorbed by Vegetation from Bidirectional Reflectance Measurements. Remote Sens Environ 51:375–384. https://doi.org/10.1016/0034-4257(94)00114-3)
Rouse J, Haas R, Schell J, Deering D, Harlan J (1974) Monitoring the Vernal Advancement and Retrogradation (Greenwave Effect) of Natural Vegetation. NASA/GSFC Type III Final Report. Greenbelt, MD: NASA/ GSFC. https://ntrs.nasa.gov/citations/19740022555
Roy P, Ravan S (1996) Biomass estimation using satellite remote sensing data—an investigation on possible approaches for natural forest. J Biosci 21(4):535–561
Singh T, Das S (2014) Predictive analysis for vegetation biomass assessment in Western Ghat Region (WG) using geospatial techniques. J Indian Soc Remote Sens 42(3):549–557
Sousa A, Gonçalves A, Mesquita P, da Silva J (2015) Biomass estimation with high resolution satellite images: a case study of Quercus rotundifolia. ISPRS J Photogramm Remote Sens 101:69–79
Sun G, Ranson K, Kharuk V (2002) Radiometric slope correction for forest biomass estimation from SAR data in the western Sayani Mountains. Siberia Remote Sens Environ 79(2–3):279–287
Thenkabail P, Stucky N, Griscom B, Ashton M, Diels J, van der Meer B, Enclona E (2004) Biomass estimations and carbon stock calculations in the oil palm plantations of African derived savannas using IKONOS data. Int J Remote Sens 25(23):5447–5472
Wylie B, Meyer D, Tieszen L, Mannel S (2002) Satellite mapping of surface biophysical parameters at the biome scale over the North American grasslands: a case study. Remote Sens Environ 79(2–3):266–278

Xiang D, Ban Y, Su Y (2016) The cross-scattering component of polarimetric SAR in urban areas and its application to model-based scattering decomposition. Int J Remote Sens 37(16):3729–3752

Zheng D, Rademacher J, Chen J, Crow T, Bresee M, Moine J, Ryua S (2004) Estimating aboveground biomass using Landsat 7 ETM+ data across a managed landscape in northern Wisconsin, USA. Remote Sens Environ 93(3):402–411

Zhou J, Yan Guo R, Sun M et al (2017) The Effects of GLCM parameters on LAI estimation using texture values from Quickbird Satellite Imagery. Sci Rep 7:7366. https://doi.org/10.1038/s41598-017-07951-w

Zianis D, Mencuccini M (2004) On simplifying allometric analyses of forest biomass. For Ecol Manage 187(2–3):311–332